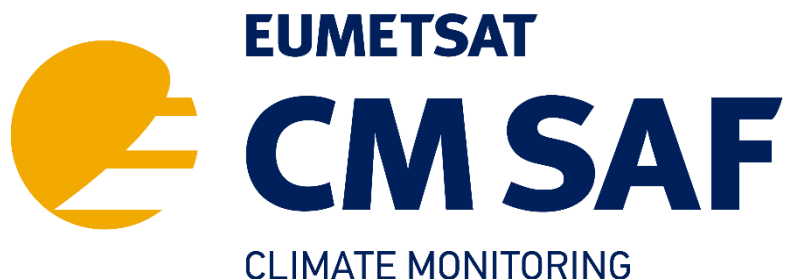


EUMETSAT Satellite Application Facility on Climate Monitoring



Validation Report

**Microwave Imager Radiance FCDR
SMMR / SSMI / SSMIS Brightness Temperatures**

DOI: 10.5676/EUM_SAF_CM/FCDR_MWI/V004

Microwave Imager Radiance FCDR R4

CM-12003

Reference Number:

SAF/CM/DWD/VAL/FCDR_MWI

Issue/Revision Index:

1.5

Date:

2022-03-31

	Validation Report Microwave Imager Radiance FCDR R4	Doc. No: SAF/CM/DWD/VAL/FCDR_MWI Issue: 1.5 Date: 2022-03-31
---	--	--

Document Signature Table

	Name	Function	Signature	Date
Author	Karsten Fennig	CM SAF Scientist		2022-03-31
Editor	Marc Schröder	Science Coordinator		2022-03-31
Approval	CM SAF Steering Group	Science Coordinator		
Release	Rainer Hollmann	Project Manager		


Distribution List

Internal Distribution	
Name	No. Copies
DWD / Archive	1
CM SAF Team	1

External Distribution		
Company	Name	No. Copies
PUBLIC		1

Document Change Record

Issue/Revision	Date	DCN No.	Changed Pages/Paragraphs
1.0	2014-11-27	SAF/CM/DWD/VAL/FCDR_SSMIS	Version for DRR 2.3.
1.1	2015-02-26	SAF/CM/DWD/VAL/FCDR_SSMIS	Final version after DRR 2.3.
1.2	2016-09-27	SAF/CM/DWD/VAL/FCDR_MWI	Version for DRR 2.13.
1.3	2016-12-06	SAF/CM/DWD/VAL/FCDR_MWI	Changes following DRR 2.13.
1.4	2022-01-31	SAF/CM/DWD/VAL/FCDR_MWI	Version for DRR 3.1
1.5	2022-03-31	SAF/CM/DWD/VAL/FCDR_MWI	Final version after DRR 3.1

	Validation Report Microwave Imager Radiance FCDR R4	Doc. No: SAF/CMDWD/VAL/FCDR_MWI Issue: 1.5 Date: 2022-03-31
---	--	---

Applicable documents

Reference	Title	Code / Validity Date
AD 1	Memorandum of Understanding between CM SAF and the Max-Planck Institute for Meteorology and Meteorological Institute, University of Hamburg	1. March 2012
AD 2	CM SAF Product Requirements Document	SAF/CM/DWD/PRD/3.8

Reference documents

Reference	Title	Code
RD 1	Algorithm Theoretical Basis Document Fundamental Climate Data Record of SSMIS Brightness Temperatures	SAF/CM/DWD/ATBD/ FCDR_SSMIS/2.2
RD 2	Algorithm Theoretical Basis Document Fundamental Climate Data Record of SSM/I Brightness Temperatures	SAF/CM/DWD/ATBD/ FCDR_SSMI/2.2
RD 3	Product User Manual Fundamental Climate Data Record of SSM/I Brightness Temperatures	SAF/CM/DWD/PUM/ FCDR_SSMI/1.2
RD 4	Validation Report Fundamental Climate Data Record of SSM/I Brightness Temperatures	SAF/CM/DWD/VAL/ FCDR_SSMI/1.2
RD 5	Product User Manual Fundamental Climate Data Record of SSMIS Brightness Temperatures	SAF/CM/DWD/PUM/ FCDR_SSMIS/1.5
RD 6	Product User Manual Fundamental Climate Data Record of SMMR Brightness Temperatures	SAF/CM/DWD/PUM/ FCDR_SMMR/1.2
RD 7	Algorithm Theoretical Basis Document Fundamental Climate Data Record of SMMR Brightness Temperatures	SAF/CM/DWD/ATBD/ FCDR_SMMR/2.2
RD 8	Requirements Review Document Microwave Imager Radiance FCDR	SAF/CM/DWD/RR/3.1

Table of Contents

I	Preface.....	7
I-1	The EUMETSAT SAF on Climate Monitoring	7
I-2	Introduction	8
II	SSM/I	9
III	SSMIS.....	9
III-3	Instrument and sensor stability.....	10
III-4	Inter-sensor evaluation of brightness temperature differences	14
III-4.1	Data sets for comparison.....	14
III-4.2	Visual inspection	14
III-4.3	Evaluation strategy.....	17
III-4.4	Inter-Sensor Evaluation Results.....	19
III-5	Comparison against GMI	35
IV	SMMR	40
IV-1	Instrument and sensor stability.....	40
IV-2	Instrument evaluation	42
V	Evaluation of brightness temperature differences against reanalysis.....	46
V-7	Evaluation results.....	47
VI	Conclusions.....	61
VII	References.....	63
VIII	Glossary.....	65

List of Tables

Table III-1: SSMIS FCDR instrument data availability at CM SAF.....	9
Table III-2: Requirement values for the SSMIS brightness temperatures product CM-12003 as given in the Product Requirements Document [AD 2].....	17
Table III-3: Statistics of the ensemble anomalies for SSMIS channel 19v GHz. The first block shows the original RDR with EIA normalized, the second block the CM SAF FCDR and the last block the CSU FCDR.....	22
Table III-4: Statistics of instrument differences for SSMIS channel 19v GHz. The numbers represent percentiles of absolute differences less than 1K, 2K, and 3K of all monthly mean grid boxes between two instruments.....	22
Table III-5: Statistics of the ensemble anomalies for SSMIS channel 19h GHz. The first block shows the original RDR with EIA normalized, the second block the CM SAF FCDR and the last block the CSU FCDR.....	24
Table III-6: Statistics of instrument differences for SSMIS channel 19h GHz. The numbers represent percentiles of absolute differences less than 1K, 2K, and 3K of all monthly mean grid boxes between two instruments.....	24
Table III-7: Statistics of the ensemble anomalies for SSMIS channel 22v GHz. The first block shows the original RDR with EIA normalized, the second block the CM SAF FCDR and the last block the CSU FCDR.....	26
Table III-8: Statistics of instrument differences for SSMIS channel 22v GHz. The numbers represent percentiles of absolute differences less than 1K, 2K, and 3K of all monthly mean grid boxes between two instruments.....	26
Table III-9: Statistics of the ensemble anomalies for SSMIS channel 37v GHz. The first block shows the original RDR with EIA normalized, the second block the CM SAF FCDR and the last block the CSU FCDR.....	28
Table III-10: Statistics of instrument differences for SSMIS channel 37v GHz. The numbers represent percentiles of absolute differences less than 1K, 2K, and 3K of all monthly mean grid boxes between two instruments.....	28
Table III-11: Statistics of the ensemble anomalies for SSMIS channel 37h GHz. The first block shows the original RDR with EIA normalized, the second block the CM SAF FCDR and the last block the CSU FCDR.....	30
Table III-12: Statistics of instrument differences for SSMIS channel 37h GHz. The numbers represent percentiles of absolute differences less than 1K, 2K, and 3K of all monthly mean grid boxes between two instruments.....	30
Table III-13: Statistics of the ensemble anomalies for SSMIS channel 91v GHz. The first block shows the original RDR with EIA normalized, the second block the CM SAF FCDR and the last block the CSU FCDR.....	32
Table III-14: Statistics of instrument differences for SSMIS channel 91v GHz. The numbers represent percentiles of absolute differences less than 1K, 2K, and 3K of all monthly mean grid boxes between two instruments.....	32

Table III-15: Statistics of the ensemble anomalies for SSMIS channel 91h GHz. The first block shows the original RDR with EIA normalized, the second block the CM SAF FCDR and the last block the CSU FCDR..... 34

Table III-16: Statistics of instrument differences for SSMIS channel 91h GHz. The numbers represent percentiles of absolute differences less than 1K, 2K, and 3K of all monthly mean grid boxes between two instruments..... 34

Table IV-1: Statistics for the SMMR FCDR channel brightness temperature anomalies. 45

Table V-1: Estimated trends for global monthly mean differences between the simulated brightness temperatures from ERA-20c and ERA5 and the combined inter-calibrated FCDR..... 48

List of Figures

Figure III-1: Time series of DMSP platform mean local equator crossing times (top), altitude (middle) and Earth Incidence Angles (EIA) of the 91 GHz imager feedhorn (bottom) for all SSMIS instruments. Thin lines are the mean values at the ascending equator crossing and thick lines depict complete orbit mean values. Colours are as follows: F16 orange, F17 blue, F18 black. 11

Figure III-2: Time series of SSMIS sensor diagnostics: Temperature of the warm calibration target (upper panel) and temperature of the reflector arm (lower panel). The grey lines denote 0°C (for colours see Figure III-1). 12

Figure III-3: Time series of SSMIS sensor diagnostics: Radiometer sensitivities for the channels at 19v, 19h, 22v, 37v, 37h, 91v and 91h GHz. The grey lines denote the specification values. 13

Figure III-4: Climatological mean of TB differences at 19 GHz between SSM/I F13 and SSMIS F16. The left column shows the original uncorrected, EIA normalised raw data records without additional modifications. The middle column depicts the CM SAF FCDR and the right column shows the CSU FCDR with all respective correction applied. The top row shows the vertical polarisation, the middle row the horizontal polarisation and the bottom row depicts the double differences between both polarisations. 15

Figure III-5: As Figure III-4 but for the SSMIS TB differences at 19 GHz between F17 and F18. 16

Figure III-6: Time series of ensemble anomalies and variability for SSM/I & SSMIS channel 19v GHz. In the upper two panels the solid lines are PM orbits and the dashed lines AM orbits. The lower panels depict daily means of AM and PM orbits. The grey lines depict the ensemble spread. Horizontal grey lines denote the optimal and target bias. For a detailed description see text (section III-4.3). Colours are as in Figure III-1 plus green (F13) and purple (F14). 21

Figure III-7: Same as Figure III-6, but for SSM/I & SSMIS channel 19h GHz..... 23

Figure III-8: Same as Figure III-6, but for SSM/I & SSMIS channel 22v GHz..... 25

Figure III-9: Same as Figure III-6, but for SSM/I & SSMIS channel 37v GHz..... 27

Figure III-10: Same as Figure III-6, but for SSM/I & SSMIS channel 37h GHz. 29

Figure III-11: Same as Figure III-6, but for SSMIS channel 91v GHz..... 31

Figure III-12: Same as Figure III-6, but for SSMIS channel 91h GHz. 33

Figure III-13: Time series of global monthly mean anomalies of SSMIS minus GMI brightness temperatures at 22 GHz. The upper panel shows the homogenised data records and the lower panel depicts the inter-sensor calibrated SSMIS data record. Colours are as in Figure III-1.	36
Figure III-14: Time series of global monthly mean anomalies of SSMIS minus GMI brightness temperatures at 19 GHz. The upper two panels show the homogenised data records and the two lower panels depict the inter-sensor calibrated SSMIS data record. Colours are as in Figure III-1.	37
Figure III-15: Time series of global monthly mean anomalies and SSMIS minus GMI channels at 37 GHz. The upper two panels show the homogenised data records and the two lower panels depict the inter-sensor calibrated SSMIS data record. Colours are as in Figure III-1.	38
Figure III-16: Time series of global monthly mean anomalies and SSMIS minus GMI channels at 91 GHz. The upper two panels show the homogenised data records and the two lower panels depict the inter-sensor calibrated SSMIS data record. Colours are as in Figure III-1.	39
Figure IV-1: Time series of Nimbus-7 local equator crossing time (a), data coverage (b), platform altitude (c), platform attitude angles (d), and Earth incidence angles (e). Thin dotted lines are the mean values at the ascending equator crossing and thick lines depict complete orbit mean values.....	41
Figure IV-2: Time series of various instrument calibration temperature readings for the 18h channel (a) and radiometer sensitivities NEdT (b) for the SSM/I like channels.	42
Figure IV-3: Time series of global monthly mean anomalies between observed and modelled TBs before (dashed lines) and after (solid lines) inter-calibration of SMMR for all FCDR channels. (SMMR, green; F08 orange).	44
Figure V-1: Time series of global monthly mean TB differences for the 19v GHz channel between the FCDR and ERA 20C (first two panels) and between FCDR and ERA5 (last two panels). Colours for the instrument are SMMR (green), F08 (orange), F10 (blue), F11 (black), F13 (green), F14 (violet), F15 (red), F16 (orange), F17 (blue), F18 (black).	50
Figure V-2: Same as Figure V-1 but for 19h GHz.	51
Figure V-3: Same as Figure V-1 but for 22v GHz.....	52
Figure V-4: Same as Figure V-1 but for 37v GHz.....	53
Figure V-5: Same as Figure V-1 but for 37h GHz.	54
Figure V-6: Same as Figure V-1 but for 85v GHz.....	55
Figure V-7: Same as Figure V-1 but for 85h GHz.	56
Figure V-8: Same as Figure V-1 but for 91v GHz.....	57
Figure V-9: Same as Figure V-1 but for 91h GHz.	58
Figure V-10: Time series of robust standard deviation of global monthly mean TB differences for the channels 19v, 22v, 37v, and 85v GHz between the CM SAF FCDR and ERA 20C	59
Figure V-11: Time series of robust standard deviation of global monthly mean TB differences for the channels 19v, 22v, 37v, and 85v GHz between the CM SAF FCDR and ERA5.	60

	Validation Report Microwave Imager Radiance FCDR R4	Doc. No: SAF/CMDWD/VAL/FCDR_MW Issue: 1.5 Date: 2022-03-31
---	--	--

I Preface

I-1 The EUMETSAT SAF on Climate Monitoring

The importance of climate monitoring with satellites was recognized in 2000 by EUMETSAT Member States when they amended the EUMETSAT Convention to affirm that the EUMETSAT mandate is also to “contribute to the operational monitoring of the climate and the detection of global climatic changes”. Following this, EUMETSAT established within its Satellite Application Facility (SAF) network a dedicated centre, the SAF on Climate Monitoring (CM SAF; <http://www.cmsaf.eu/>).

The consortium of CM SAF currently comprises the Deutscher Wetterdienst (DWD) as host institute, and the partners from the Royal Meteorological Institute of Belgium (RMIB), the Finnish Meteorological Institute (FMI), the Royal Meteorological Institute of the Netherlands (KNMI), the Swedish Meteorological and Hydrological Institute (SMHI), the Meteorological Service of Switzerland (MeteoSwiss), and the Meteorological Service of the United Kingdom (UK MetOffice) and the Centre National de la Recherche Scientifique, Laboratoire d’études en Géophysique et Océanographie Spatiales, France (CNRS, LEGOS). Since the beginning in 1999, the EUMETSAT Satellite Application Facility on Climate Monitoring (CM SAF) has developed and will continue to develop capabilities for a sustained generation and provision of Climate Data Records (CDR’s) derived from operational meteorological satellites.

In particular the generation of long-term data sets is pursued. The ultimate aim is to make the resulting data sets suitable for the analysis of climate variability and potentially the detection of climate trends. CM SAF works in close collaboration with the EUMETSAT Central Facility and liaises with other satellite operators to advance the availability, quality and usability of Fundamental Climate Data Records (FCDRs) as defined by the Global Climate Observing System (GCOS). As a major task the CM SAF utilizes FCDRs to produce records of Essential Climate Variables (ECVs) as defined by GCOS. Thematically, the focus of CM SAF is on ECVs associated with the global energy and water cycle.

The CM SAF data sets can serve applications related to the new Global Framework of Climate Services initiated by the WMO World Climate Conference-3 in 2009. CM SAF is supporting climate services at national meteorological and hydrological services (NMHSs) with long-term data records but also with data sets produced close to real time that can be used to prepare monthly/annual updates of the state of the climate. Both types of products together allow for a consistent description of mean values, anomalies, variability, and potential trends for the chosen ECVs. CM SAF ECV data sets also serve the improvement of climate models both at global and regional scale.

A catalogue of all available CM SAF products is accessible via the CM SAF webpage, <https://www.cmsaf.eu/>. Here, detailed information about product ordering, add-on tools, sample programs and documentation is provided.

I-2 Introduction

This CM SAF validation report provides information on the evaluation of the Fundamental Climate Data Record (FCDR) of microwave brightness temperatures from the conical scanning microwave sensors Special Sensor Microwave/Imager (SSM/I), Special Sensor Microwave Imager/Sounder (SSMIS) and Scanning Multichannel Microwave Radiometer (SMMR). This fourth release is a continuation of the previous release (available from CM SAF; http://dx.doi.org/10.5676/EUM_SAF_CM/FCDR_MWI/V003).

Data from the space-borne microwave imagers and sounders such as the Scanning Multichannel Microwave Radiometer (SMMR), Special Sensor Microwave/Imager (SSM/I) and the Special Sensor Microwave Imager/Sounder (SSMIS) are used for a variety of applications, such as analyses of the hydrological cycle (precipitation and evaporation) and related atmospheric and surface parameters, as well as remote sensing of sea ice, soil moisture, and land surface temperatures. Carefully calibrated and homogenised radiance data sets are a fundamental prerequisite for climate analysis, climate monitoring and reanalysis. Several National Meteorological Services and Reanalysis centres assimilate microwave radiances directly and not derived geophysical parameters. Forecast and reanalysis can thus benefit from a Fundamental Climate Data Record (FCDR) of brightness temperatures (Poli et al. 2015). The generation of Thematic Climate Data Records (TCDRs) strongly relies on the availability of FCDRs. Highest possible TCDR quality can be achieved easiest in radiance space, in turn increasing the products value for users.

The predecessors of this data record and the data processor suite have originally been developed at the Max-Planck Institute for Meteorology (MPI-M) and the University of Hamburg (UHH) for the Hamburg Ocean Atmosphere Parameters and Fluxes from Satellite Data (HOAPS, <http://www.hoaps.org/>) climatology. HOAPS is a compilation of climate data records for analysing the water cycle components over the global oceans derived from satellite observation (Andersson et al. 2011). The main satellite instrument employed to retrieve the geophysical parameters is the SSM/I and much work has been invested to process and carefully homogenize all SSM/I instruments onboard the Defence Meteorological Satellite Program (DMSP) platforms F08, F10, F11, F13, F14 and F15 (Andersson et al., 2010).

The HOAPS processing suite has been transferred to CM SAF in a Research to Operations activity in order to provide a sustained processing of the climate data records which is one of the main tasks of CM SAF, but not in the focus of the research group at the MPI-M / UHH. The operational processing and reprocessing of the FCDRs and TCDRs as well as the provision to the research community is maintained and coordinated by the CM SAF.

The first release of the CM SAF FCDR (Fennig et al. 2013) focussed on the SSM/I series, covering the time period from 1987 to end of 2008. This FCDR has already been used in the ESA CCI Sea ice project and in the reanalysis ERA5. In order to continue the HOAPS TCDRs beyond 2008 it was necessary to extend the underlying FCDR of microwave TBs with the SSMIS sensor family aboard the DMSP platforms F16, F17, and F18, which was accomplished with the second release of the CM SAF FCDR (Fennig et al. 2015). This combined FCDR of SSM/I and SSMIS brightness temperatures provides a consistent FCDR from 1987 to 2013.

Following requests from users of the FCDR, the third release focussed on the extension of the microwave brightness temperature data record to the earlier time period from 1978 to 1987 with observations from the SMMR on-board Nimbus-7. However, this turned out to be a very challenging task, as it has not been possible to get hold of the original raw instrument data records. Although this data record must have eventually been transferred from the Marshall Space Flight Centre (MSFC) to the National Snow & Ice Data Center (NSIDC), it is currently not available from their archives. Instead, the Nimbus-7 SMMR Pathfinder Level 1B Brightness Temperatures data record, available from NSIDC (Njoku, 2003), is used to generate this FCDR.

With the fourth release of the Microwave Imager Radiance FCDR, the temporal coverage of the SSMIS will be extended to 31 December 2020 while the SMMR and SSM/I data records remain unchanged. The data records for the SSMIS sensors on-board F16, F17, and F18 have been reprocessed for this fourth FCDR release, implementing significant improvements. The same algorithm and processing tools are used for R4 of SSM/I and SMMR data as for the predecessor CM-12002. A detailed list of changes for this release is available in the corresponding ATBD for the SSMIS component [RD 1].

II SSM/I

The SSM/I component of this combined FCDR remains unchanged compared to the previous third release. The corresponding documents ATBD [RD 2], Product User Manual [RD 3], and Validation Report [RD 4] are available as separate documents. These documents are also available directly from our website at <https://www.cmsaf.eu/docs>.

III SSMIS

The CM SAF FCDR from SSMIS brightness temperatures is compiled as daily collections of all observations from each sensor. All sensor specific data available in the raw data records are provided as well as additional information like quality control flags, Earth incidence angles (EIA), averaged 91 GHz brightness temperatures, synthetic 85 GHz brightness temperatures, incidence angle normalisation offsets, solar calibration correction offsets, and inter-sensor calibration offsets. The new SSMIS FCDR is available for the time period from November 2005 until December 2020. A detailed list of data availability for each of the three SSMIS platforms is given in Table III-1.

A technical description of the data set, including information on the file format as well as on the data access is provided in the corresponding Product User Manual [RD 5]. Furthermore details on the CM SAF inter-sensor calibration model, the implementation of the processing chain and individual processing steps are described in the SSMIS Algorithm Theoretical Basis Document

Table III-1: SSMIS FCDR instrument data availability at CM SAF.

DMSP platform	Launch date	Record start	Record end
F16	2003-10-18	2005-11-01	2020-12-31
F17	2006-11-04	2006-12-14	2020-12-31
F18	2009-10-18	2010-03-08	2020-12-31

[RD 1]. Basic accuracy requirements are defined in the product requirements document [AD 2]. An extensive description of the SSMIS instrument and satellite characteristics can be found in Kunkee et al. (2008).

III-3 Instrument and sensor stability

Figure III-1 shows the time series of the mean DMSP platform local equator crossing times, altitude and the Earth Incidence Angles (EIA) of the 91 GHz feedhorn for the different SSMIS instruments. The local overpass time is not constant for all platforms. The strongest drift can be observed for DMSP F16 and F18 from 8 to 4 AM/PM, while DMSP F17 depicts a more constant equator crossing time around 6 AM/PM. Due to this drift in the local overpass time, the brightness temperature (TB) differences between the instruments are not constant and the diurnal cycle variation must be taken into account during the inter-sensor calibration and when comparing the inter sensor differences.

The altitude of the satellite platforms remains very constant over time, as depicted in the Figure III-1, middle panel. Due to varying alignments of the imager feedhorn on the different platforms, the mean EIA ranges between 52.9 to 53.3 degrees (Figure III-1, lower panel). The mean orbit EIA remains constant for SSMIS_{F16} and SSMIS_{F17}. The mean EIA of F18 increases in May 2011 due to a changed platform pitch angle. The SSMIS_{F18} depicts an artificial trend in the v-pol channels, as documented in the validation report of the FCDR release R2 (Fennig et al., 2015). The most likely scenario is a change in the attitude pitch angle. Though undocumented in the available literature but corrected for also by CSU, the pitch angle was changed in the processing software from FCDR release R3 onwards to remove the observed bias.

The regular seasonal variation of the local EIA at equator crossing is caused by the orbit precession and can also lead to differences up to 0.2 degree in EIA. Since a change of 0.1 degree in EIA will change the vertical polarized TB up to 0.2 K, these variations must be taken into account by normalizing the observed TBs to a constant EIA. The CM SAF FCDR data files contain offsets, which are computed using the Furhop and Simmer (1996) algorithm to normalize the TBs to constant 53 degree EIA. This TB offset can be applied if the user's application is designed for constant zenith angles and is only valid over ocean.

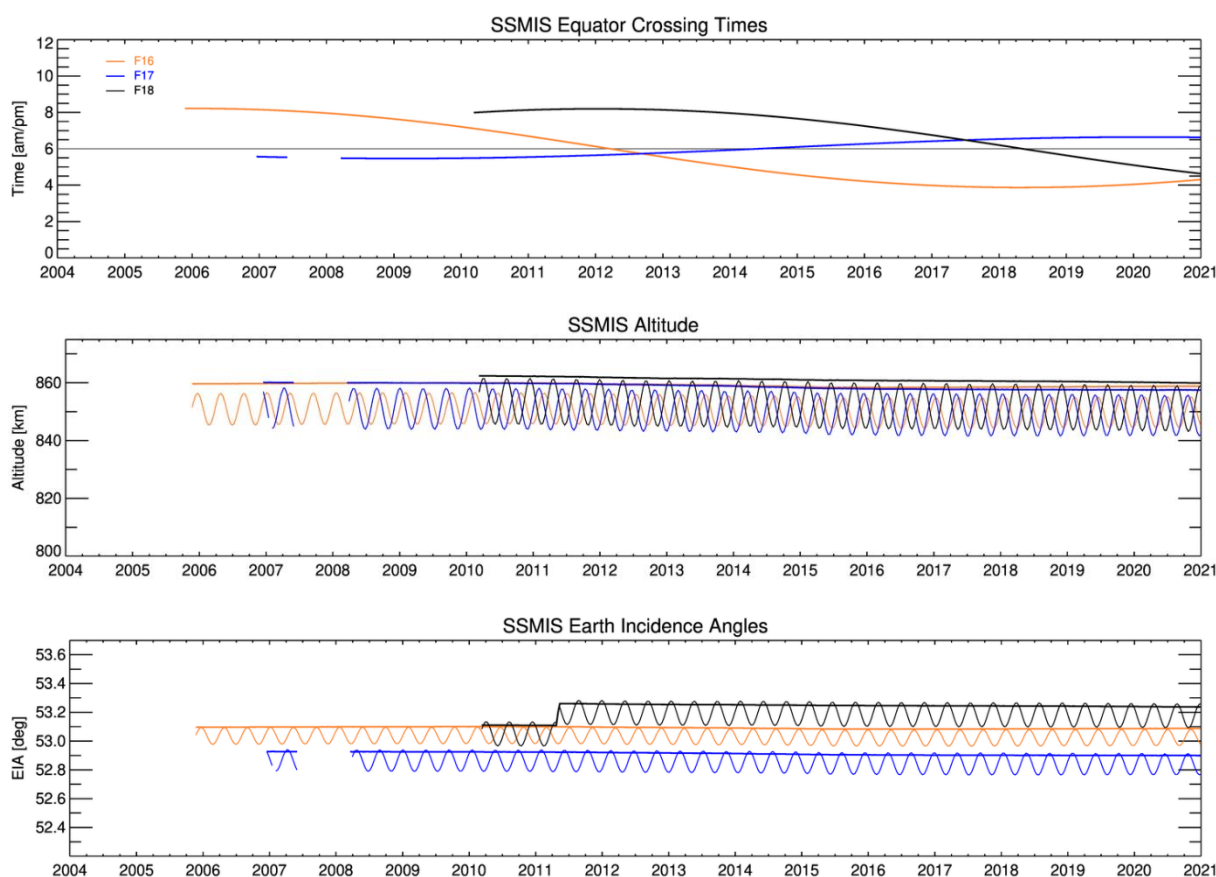


Figure III-1: Time series of DMSP platform mean local equator crossing times (top), altitude (middle) and Earth Incidence Angles (EIA) of the 91 GHz imager feedhorn (bottom) for all SSMIS instruments. Thin lines are the mean values at the ascending equator crossing and thick lines depict complete orbit mean values. Colours are as follows: F16 orange, F17 blue, F18 black.

Figure III-2 shows the time series of hot load target temperatures and reflector arm temperatures for all three SSMIS instruments. The temperature of the warm calibration target remains very constant at about 310 K. Only two short events can be observed in 2018 for the SSMIS_{F18}, where the mean warm target temperature drops to 290 K. This is a clear improvement over the SSM/I design, where a strong seasonal variability reaching an amplitude of up to 50 K was observed (see also the SSM/I validation report [RD 4]). The variation in the reflector arm temperature is an important indicator for the correction of the SSMIS reflector emissivity problem. The temperature depends on the amount of time spent in the Earth shadow during an orbit and thus on the local equator overpass time. This dependency can be observed from the change in the seasonal arm temperature variations of SSMIS_{F16} and SSMIS_{F18}, when the overpass time drifts from 8 to 4 AM/PM. In the beginning the seasonal variation in the warm target temperature is very small, but starts to undergo strong cooling events from 2011 (2017) onward, when the local overpass time has drifted before 7 AM/PM. The minima in the arm temperatures are occurring at solar equinox in spring and autumn. When SSMIS_{F17} and SSMIS_{F16} are at the same overpass time in 2012, the seasonal arm temperature variations are nearly identical. This can also be observed for SSMIS_{F17} and SSMIS_{F18} in 2017/2018. In 2014 the SSMIS_{F16} cooling events fade away, when the local overpass time is before 5 AM/PM.

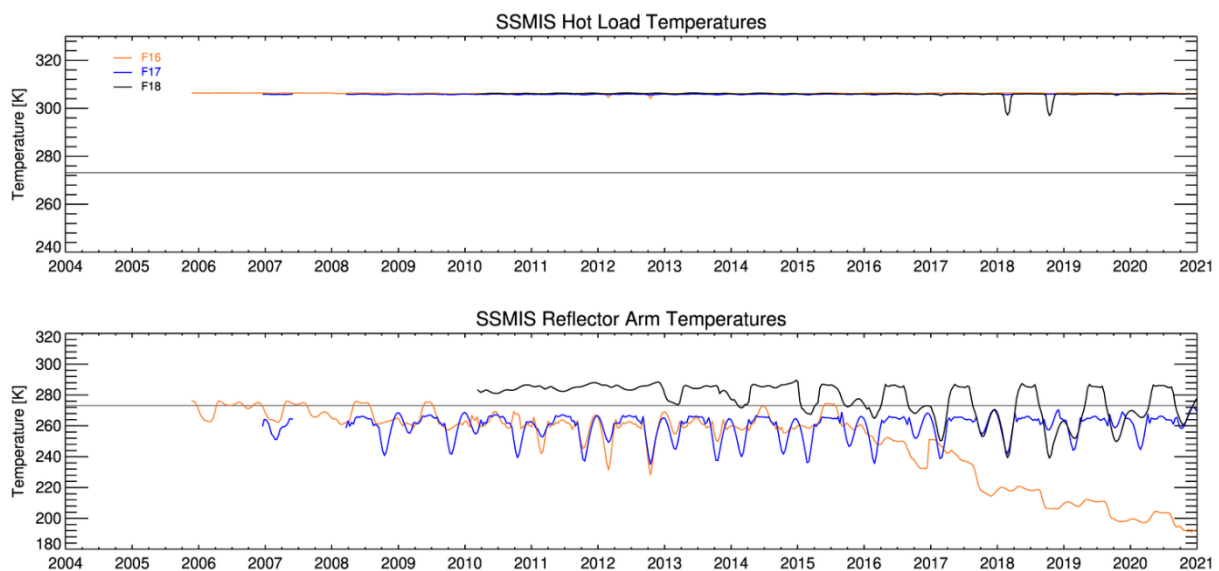


Figure III-2: Time series of SSMIS sensor diagnostics: Temperature of the warm calibration target (upper panel) and temperature of the reflector arm (lower panel). The grey lines denote 0°C (for colours see Figure III-1).

A very strong decrease can be observed for SSMIS_{F16} from 2016 onwards. The mean SSMIS_{F16} arm temperature drops to 190 K at the end of 2020. As the SSMIS_{F16} has an emissive reflector, this strong trend would be detectable in the un-corrected TBs. However, after applying the emissivity correction, an artificial trend in the TBs at 91 GHz was observed, leading to the conclusion that the temperature sensor of the SSMIS_{F16} reflector operates erroneously since 2016. The SSMIS emissivity correction procedure was modified to account for this issue (see the SSMIS ATBD for more details [RD 1]). However, this correction has an impact on the quality of the TBs after 2016.

Figure III-3 shows the time series of the radiometer sensitivities for all SSM/I-like channels. The radiometer noise equivalent differential temperature ($NEdT$) is estimated at the warm calibration target temperature (see the corresponding ATBD [RD 1]) and is available as a daily mean value from the CM SAF FCDR data files for all SSMIS channels. Overall, the radiometer noise is within the specification for most of the channels. The most pronounced feature of the SSMIS_{F18} is a sharp increase in the noise level in early 2012, visible in all channels. The maximum impact can be observed in the 37h channel, showing an increase from 0.4 K to 0.8 K. Also an overall increase in the noise level in 2015 and 2020 can be detected for SSMIS_{F18}. Again, the 37h channel is affected at most, reaching the design specification at the end of 2015 and exceeding the specification in 2020. All SSMIS_{F17} channels behave inconspicuously. Both 91 GHz channels of the SSMIS_{F16} are affected by a strong anomaly in summer 2015. The most problematic channel is the 91h channel of the SSMIS on-board F16. It is above the specification for most of the time and depicts a very noisy behaviour. The $NEdT$ stays within the specification noise level only in 2014 and 2017.

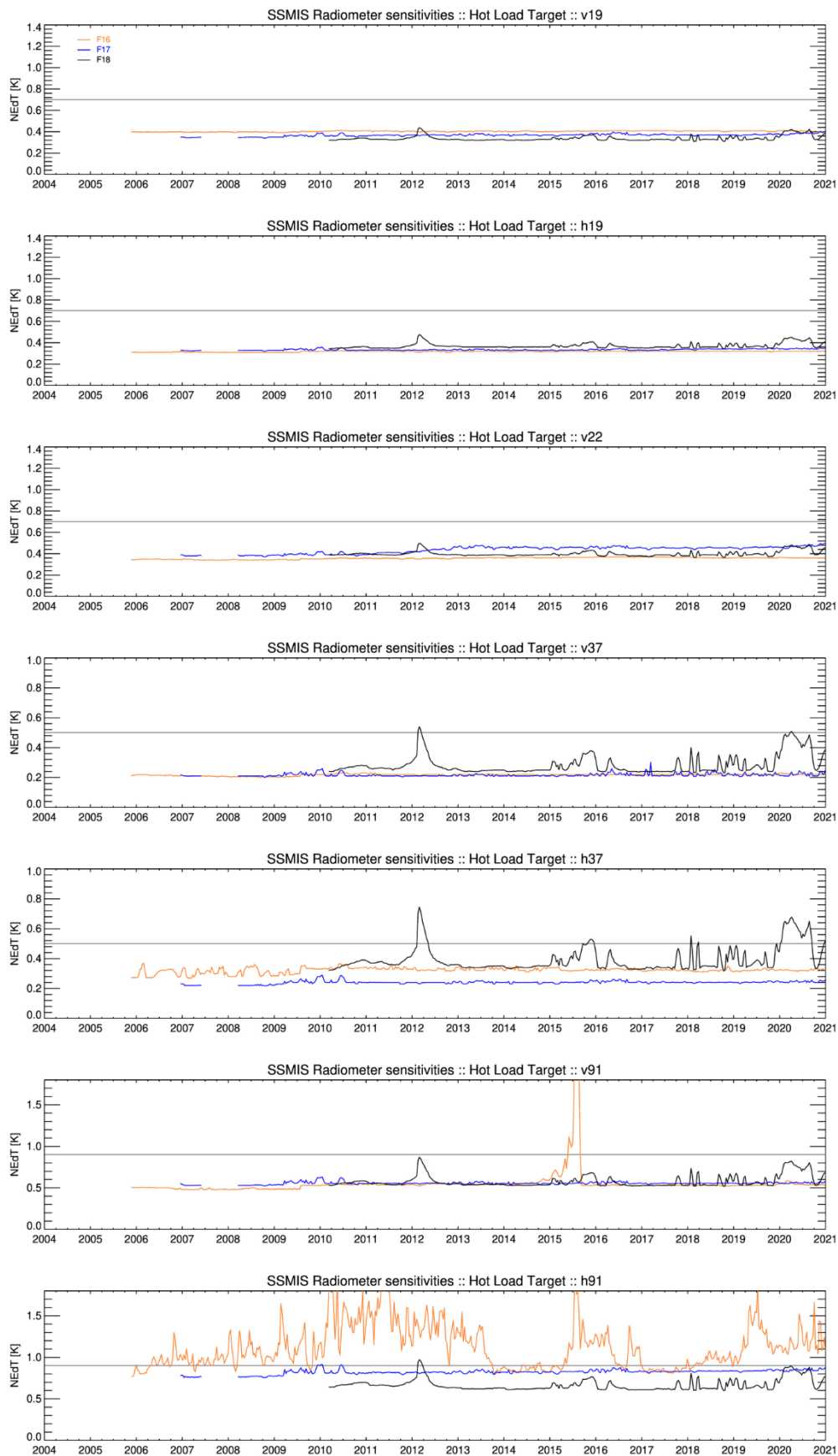


Figure III-3: Time series of SSMIS sensor diagnostics: Radiometer sensitivities for the channels at 19v, 19h, 22v, 37v, 37h, 91v and 91h GHz. The grey lines denote the specification values.

	<p style="text-align: center;">Validation Report Microwave Imager Radiance FCDR R4</p>	<p>Doc. No: SAF/CMDWD/VAL/FCDR_MW Issue: 1.5 Date: 2022-03-31</p>
---	---	---

III-4 Inter-sensor evaluation of brightness temperature differences

The purpose of a validation is to establish, that the measurement under scrutiny agrees with an independent, and (ideally) traceable, measurement or estimate, within the combined measurement uncertainties in both. A conclusion from the error budget estimation (see ATBD [RD 1]) is, that a complete comprehensive validation of the SMMR / SSM/I / SSMIS brightness temperatures is not possible, as there is no absolute validation reference available. The final aim of an evaluation process must be to show that the measured brightness temperatures are in agreement with modelled brightness temperatures within the expected random uncertainties. As a major requisite, a Fundamental Climate Data Record must show improved quality compared to the existing Raw Data Records (RDR) in order to be a useful data set, providing added value to the user community.

Hence, the main validation strategy in this document is to compare this FCDR of SSMIS brightness temperatures to the original RDR and to another data record (CSU SSMIS FCDR (Berg, 2013)), in order to quantify the quality of the inter-sensor calibration and to compare the different inter-sensor calibration approaches. The aim of this validation report is to show that the homogeneity of the reprocessed FCDR is significantly improved compared to the original raw Temperature Data Records.

Additionally to this inter-sensor comparison, a comparison of SSMIS observation against GM brightness temperatures is presented in section III-5. Finally, also a comparison against modelled brightness temperatures, using two different reanalysis data sets, is conducted in section V in order to analyse the stability of the final FCDR across the platforms.

III-4.1 Data sets for comparison

Another FCDR of SSMIS brightness temperature has been released from Colorado State University (CSU). The inter-sensor calibration model used for this data set is described in detail in Sapiano and Berg (2013) and Berg and Sapiano (2012). The CSU inter-calibration model uses the SSM/I_{F13} as reference instrument. The inter-calibration is implemented in a two-step process. First a matchup database against rain-free TMI observation over ocean is used to correct for solar intrusion effects. This data base consists of double differences (SSMIS-model)-(TMI-model) as a function of solar azimuth, solar elevation, and scene temperature. After this correction to TMI has been applied, the SSMIS TBs are inter-calibrated to the SSM/I_{F13} using the mean of different types of double differences. The scene dependence is solved via a look-up table with fixed tie-points. For TBs outside the covered range, the maximum and minimum values are applied respectively.

III-4.2 Visual inspection

Before evaluating the TB differences statistically, a visual inspection of brightness temperature differences for all satellite pairs has been done to test the performance of the inter-sensor calibration models over all surface types. The warmest TBs over land are not used directly during the inter-calibration model fitting procedure of the CM SAF FCDR due to the strong diurnal cycle of the land surface. As the overpass time between the satellites differs by up to

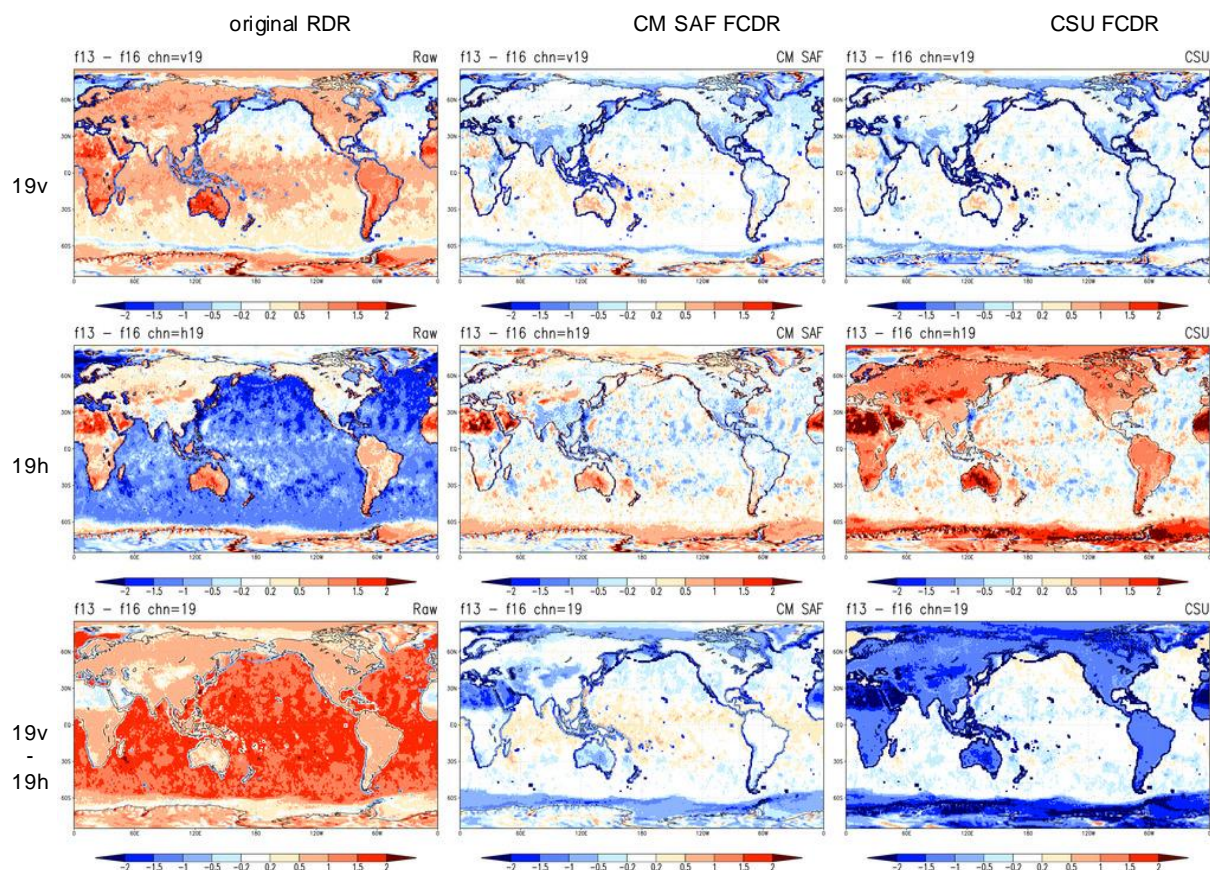


Figure III-4: Climatological mean of TB differences at 19 GHz between SSM/I F13 and SSMIS F16. The left column shows the original uncorrected, EIA normalised raw data records without additional modifications. The middle column depicts the CM SAF FCDR and the right column shows the CSU FCDR with all respective correction applied. The top row shows the vertical polarisation, the middle row the horizontal polarisation and the bottom row depicts the double differences between both polarisations.

three hours, significant differences in the observed brightness temperature are to be expected over land surfaces. The main challenge for the inter-calibration model is to keep the natural variability unchanged and to only correct for instrument related biases. The mean diurnal variability over land is assumed to be independent of the polarization at a given frequency. Thus, a double differencing technique $(TB_{V_S1} - TB_{V_S2}) - (TB_{H_S1} - TB_{H_S2})$ is applied to remove the diurnal effects. No or small residual biases should thus remain for the inter-calibrated sensors. As the result of these comparisons, two examples are presented in Figure III-4 and Figure III-5. The figures show the climatological daily means (AM and PM) of TB differences at 19 GHz between SSM/I_{F13} and SSMIS_{F16} (Figure III-4) and between SSMIS_{F17} and SSMIS_{F18} (Figure III-5). The first example is of major importance, because SSMIS_{F16} is defined as the transfer target from the SSM/I to the SSMIS era.

The uncorrected raw data (Figure III-4, left column) show a strong scene dependent bias between SSM/I_{F13} and SSMIS_{F16}. The overpass time difference between the satellites is less than 2 hours. Therefore, negative anomalies should be visible over land areas for the vertical and horizontal polarization, where a diurnal cycle is expected. No significant differences over the ocean are expected. However, these anticipated features are not depicted in the uncorrected data. The FCDRs from CM SAF (middle column) as well as from CSU (right column) both remove the observed inter-sensor differences over the oceans. The remaining

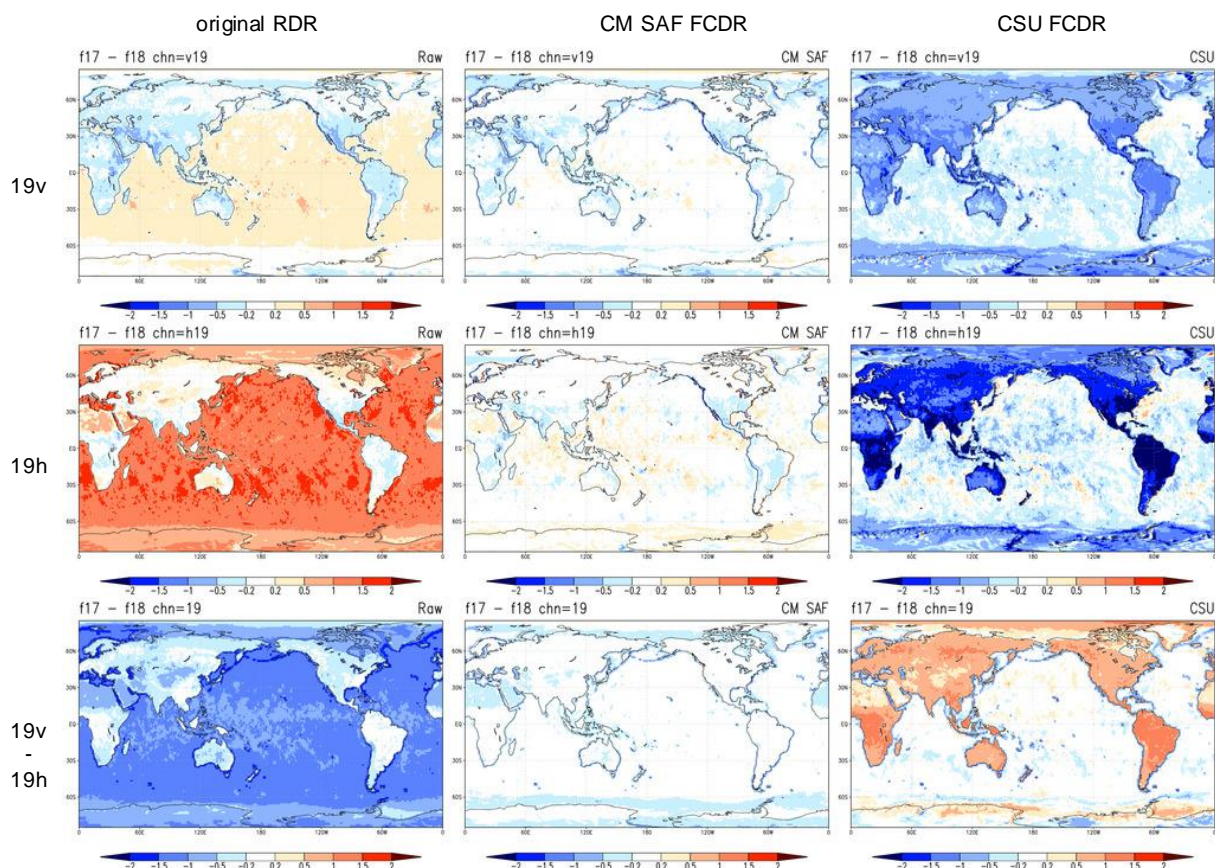


Figure III-5: As Figure III-4 but for the SSMIS TB differences at 19 GHz between F17 and F18.

anomalies in the CM SAF FCDR show small negative values over the northern oceanic areas and small positive values for the southern oceans. Vertical and horizontal polarizations depict, as expected, a similar diurnal pattern after correction and no significant residual biases appear in the double difference plot (middle column, bottom panel) over the ocean. The CM SAF FCDR also shows small biases over the Sahara desert and snow and ice-covered areas, which are due to missing incidence angle corrections for these surface types. The larger differences over the coast lines and sea-ice edges are caused by the gridding procedure (filtering of mixed surface types) and are artificial.

However, for the CSU FCDR very strong differences remain in the double difference image over land surfaces and sea-ice (right column, bottom panel). In this case, the inter-sensor calibration procedure completely removes the differences over ocean and land from the 19v channel (right column, top panel). Positive anomalies remain for the 19h channel (right column, middle panel) over land, whereas small negative anomalies are to be expected due to the diurnal warming of the land surface. Also, a precipitation pattern is visible in the difference of the channel 19h. This observed bias is most likely caused by an underestimation of the scene dependence of the 19h channel corrections. The CSU inter-calibration coefficients are determined over the TRMM covered area ($\pm 40^\circ$ latitude), using only rain-free observation over ocean. This limits the utilized spectrum to the radiometric cold end, while excluding all radiometric warm targets and thus existing scene dependences are underestimated.

Figure III-5 shows the differences between $SSMIS_{F17}$ and $SSMIS_{F18}$ for the 19 GHz channels. The overpass time difference is larger than for F13/F16 at the beginning, with DMSP F18

observing two hours later than DMSP F17, and slowly decreasing over time. In 2017 both platforms have the same overpass time and at the end of 2020, DMSP F18 is eventually two hours earlier than DMSP F17. Hence, the residual warm biases over land should nearly cancel out, when averaged over the whole time period. While the CM SAF FCDR shows only small remaining differences, the CSU FCDR does not depict such a consistent behaviour. The differences for the horizontal polarization (right column, middle panel) over land are considerable larger than for the vertical polarization (right column, top panel). This leads to a significant positive residual bias over radiometric warm surfaces (sea ice, land) in the comparison of SSMIS_{F17} and SSMIS_{F18} (right column, bottom panel). Large scale differences between 0.2 and 0.5 K remain over the ocean for both polarisations.

The other difference maps for channels and instrument pairs not presented here, show similar results but with increasing noise at higher frequencies.

III-4.3 Evaluation strategy

Similar to the visual inspection, the CM SAF FCDR is compared to the RDR and CSU brightness temperature data set. The homogeneity of the data sets is tested by comparing against the respective ensemble mean of the available satellites in each data record and additional statistical values are given for bias, robust standard deviation (RSD), median absolute deviation (MAD) and decadal stability. The requirements for the SSMIS brightness temperature product are defined in the Product Requirements Document (PRD) [AD 2]. Table III-2 recalls these requirements for monthly global mean values.

In order to quantify the consistency of the brightness temperatures across the SSMIS sensors, a reference has to be established first. As there is no absolute reference available and the operating sensors change over time, we choose the ensemble mean of all available instruments at each month as the relative reference. This approach simplifies the further analysis, as it can be performed per sensor and not for all sensor pairs. The inter-sensor differences are derived by comparing the respective bias values to the ensemble mean. The maximum inter-sensor difference is the ensemble spread, which characterizes the observation uncertainty, because without additional information each sensor could be treated as the “true” observation.

A global monthly mean bias only characterizes the mean systematic offset to another sensor. However, it is also important to quantify the observed regional differences, which is characterized by the distribution of gridded monthly mean brightness temperature differences. The median of absolute differences (MAD), without correcting for the mean systematic offset (bias), is a measure of the total absolute uncertainty. In terms of monthly mean gridded data

Table III-2: Requirement values for the SSMIS brightness temperatures product CM-12003 as given in the Product Requirements Document [AD 2].

	Threshold	Target	Optimal
Bias	3 K	2 K	1 K
Decadal stability $t_D = 0.03 \text{ K/decade}$	Significance $\alpha \geq 0.3\%$	Significance $\alpha \geq 5\%$	Significance $\alpha \geq 30\%$

samples, a MAD of 1 K means that 50% of all grid box brightness temperature differences are within 0-1 K. A robust (resilient to outliers) measure of the statistical dispersion of a distribution is the median absolute deviation about the median. Assuming a normal distribution, the expected standard deviation can be estimated from the median absolute deviation by scaling it with a factor of 1.48. For comparison, this approach has also been applied to the CSU data set which covers the same time period as the CM SAF FCDR. Prior to consistency analysis, the data files have first been converted to the CM SAF data format. Then both data sets have been gridded to equal angle 1° monthly mean global fields separately for AM and PM orbits. For the comparisons all oceanic grid cells are used.

To evaluate the relative instrument differences, an ensemble mean data set has been compiled for each FCDR on a monthly basis for all instruments and channels. The ensemble monthly mean grid box brightness temperature $\langle T_B \rangle$ for each month t and grid box index g is calculated as the arithmetic mean of the individually gridded monthly mean brightness temperatures T_B from all available instruments s :

$$\langle T_B \rangle(t, g) = \frac{1}{N_s} \cdot \sum_{s=1}^{N_s} T_B(s, t, g), \quad \text{Equation 1}$$

with N_s as the number of contributing instruments for each grid box and month.

The distribution of brightness temperature differences ΔT_B relative to this ensemble mean

$$\Delta T_B(s, t, g) = T_B(s, t, g) - \langle T_B \rangle(t, g) \quad \text{Equation 2}$$

is then statistically analysed. Here, we apply robust statistics (see above), with M as the median of the distribution of all grid box brightness temperature differences ΔT_B for each instrument s . We define:

$$\begin{aligned} Bias_s &= M(\Delta T_B(t, g)|_s) \\ MAD_s &= M(|\Delta T_B(t, g)|_s) \\ RSD_s &= M(|Bias_s - \Delta T_B(t, g)|_s) \cdot 1.48 \end{aligned} \quad \text{Equation 3}$$

The requirement for the global monthly mean consistency between the instruments is given in Table III-2 in terms of inter-sensor biases. As $Bias_s$ is relative to the ensemble mean, the inter-sensor bias is derived as the corresponding difference $Bias_{s1} - Bias_{s2}$.

The decadal stability t_D for each channel and instrument is estimated using a linear model trend, fitted to the time series of monthly anomalies relative to the ensemble mean. The anomalies are defined as the median of the global distribution of brightness temperature differences ΔT_B :

$$\overline{\Delta T_{B,s}}(t) = M[\Delta T_B(g)|_s](t). \quad \text{Equation 4}$$

A simple model with a linear decadal trend t_D in K/decade is then defined as:

$$\overline{\Delta T_{B,s}}(t) = \overline{\Delta T_{B,s}}(t = 0) + \frac{t_D}{120} \cdot t + \varepsilon(t), \quad \text{Equation 5}$$

with $\varepsilon(t)$ representing the fraction of the monthly anomalies not explained by the linear approximation. The linear model terms (offset and trend) are found by a least square

regression fit. The stability requirement, as defined in the requirement review (Table III-2, RD 8, AD 2), is a decadal stability with a linear trend of $t_D < 0.03 \text{ K/decade}$. The requirement levels are defined in terms of significance levels of statistical hypothesis testing. The null hypothesis $t_D > 0.03 \text{ K/decade}$ can be rejected (criterion is met), if the probability of rejecting the null hypothesis is higher than the threshold (0.3%), target (5%) or optimal (30%) criterion (see Table III-2). The significance level α of the decadal trend is determined using a two-sided t-test, applying a standard uncertainty of 0.1 K from the distribution of the global monthly anomalies.

The results of the statistical analysis are shown in Figure III-6 to Figure III-12 and summarized in Table III-3 to Table III-16, grouped by channel. The tables also contain the maximum inter-sensor bias, which is the maximum absolute bias difference, computed using the first equation in Equation 3. All figure panels contain five images with time series of global monthly mean values of:

1. TB anomalies of the raw data record without any modification,
2. TB anomalies after reflector emissivity correction, EIA normalization, and diurnal cycle removed,
3. TB anomalies of the CM SAF FCDR inter-sensor calibration offsets and solar calibration correction offsets applied,
4. TB anomalies of the CSU FCDR,
5. Robust standard deviation (RSD) of CM SAF FCDR TB anomalies.

III-4.4 Inter-Sensor Evaluation Results

The time series of the raw data records plots (RDR, Figure III-6 to Figure III-12 top panel) show a very diverse picture. The agreement in the raw data records between the SSM/I is generally better than between the SSMIS. This is evident for the homogenised data records that have been corrected for reflector emissivity, incidence angle and diurnal cycle variations (RDR, Figure III-6 to Figure III-12 second panel). Most TB differences for the SSM/I instruments are below 0.5 K. The largest difference found for the SSM/I is about 1 K in the 37 GHz channels. In contrast to this, most of SSMIS differences are between 0.5 K to 1 K, with a maximum of 2 K at 91 GHz before the inter-calibration. The ensemble spread between SSM/I and SSMIS channels is larger than 3 K for the 37 GHz channels. Best agreement between both sensor types is found for the 19 GHz channels with about 1 K difference. This means, most of the observed inter-sensor differences before applying the inter-calibration offsets are larger than the estimated standard uncertainty of the SSM/I instrument, which is about 0.6 to 1 K (see ATBD [RD 1]).

The calibration enhancement due to intrusion and reflector emissivity corrections (from first to second panel) and the inter-calibration (from second to third panel) reduce the inter-sensor variations and increase the quality and stability of the SSMIS data record significantly. The global climatological mean inter-satellite bias of the SSMIS has been reduced to below 0.05 K. As for the raw data record, the agreement in the final FCDRs between the individual SSM/I instruments is generally better than between the SSMIS instruments.

Further results are summarised as follows:

- Both analysed FCDRs significantly reduce the observed differences between the monthly means and show very similar results for individual satellites. All global monthly mean inter-sensor differences are within the optimum requirement of 1 K. In terms of maximum inter-sensor bias (ensemble spread), the CM SAF FCDR is performing slightly better. Comparing the absolute maximum difference between the individual satellite biases to the ensemble mean, the CM SAF FCDR shows a remaining ensemble spread of 0.03 K, while for the CSU FCDR values up to 0.19 K remain.
- Overall, the monthly anomalies show a variability which is larger for horizontally polarized channels and increases with higher frequencies. This variability is caused by the inclusion of all scenes, i.e. no rain filtering is applied. This additional noise can be interpreted as an additional uncertainty due to differences in space and time collocation and sampling variability.
- No significant trend above the threshold criteria of 0.03 K can be detected.
- A periodic increase in the TB bias is visible in the CSU FCDR for most channels from early 2015 onwards. The ensemble spreads depict maximum offsets of about 0.5K in northern hemispheric winter. This feature is also visible in the homogenised data records (second panel). This instrument related issue is removed in the CM SAF FCDR.
- A significant anomaly above 1 K difference is found in summer 2015 in the 91 GHz channels of F16. This also corresponds to an observed increase in *NEdT* during this time period as described in section III-3 (compare also Figure III-3). Another smaller anomaly of about 1 K is visible in winter 2014 in the 91v channel. Both deviations are smaller in the CM SAF FCDR compared to the CSU FCDR.
- The robust standard deviations depict constant values over time for all channels and instruments between 0.5 K and 1 K. This means, that about 70% of all analysed monthly mean grid boxes are within ± 0.5 K to ± 1 K, respectively. The outliers above 1 K are caused by incomplete months and therefore increased variability due to a shorter sampling period.
- The RSD is slightly increased during the SSM/I and SSMIS overlap, but not significantly different.
- The statistical measures derived from both FCDRs depict a very good and similar performance of both data sets in terms of RSD and MAD. However, some channels (22v, 19h) in the CSU FCDR show a small remaining bias of about 0.2 K.
- The noise level of all instruments is very similar.
- The large seasonal variations of the TB differences at 91 GHz (first panels) are caused by the reflector emissivity issue, affecting the instruments on-board SSMIS_{F16} and SSMIS_{F17}. These anomalies are in the order of 1 K for the global mean and larger in the horizontal polarised channels. These anomalies are corrected for in the CM SAF FCDR and only small variations remain in the homogenised plots (second panels).

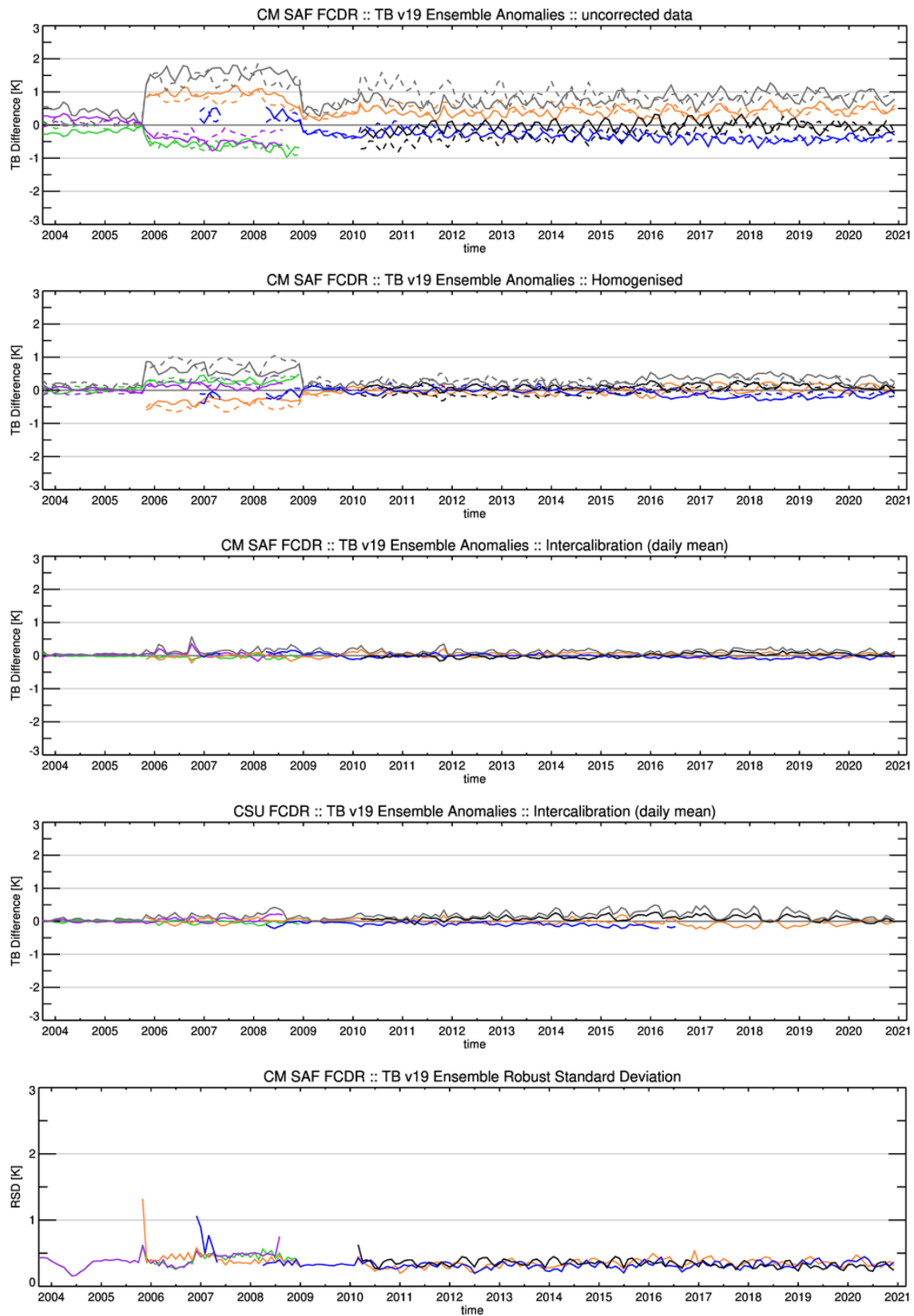


Figure III-6: Time series of ensemble anomalies and variability for SSM/I & SSMIS channel 19v GHz. In the upper two panels the solid lines are PM orbits and the dashed lines AM orbits. The lower panels depict daily means of AM and PM orbits. The grey lines depict the ensemble spread. Horizontal grey lines denote the optimal and target bias. For a detailed description see text (section III-4.3). Colours are as in Figure III-1 plus green (F13) and purple (F14).

Table III-3: Statistics of the ensemble anomalies for SSMIS channel 19v GHz. The first block shows the original RDR with EIA normalized, the second block the CM SAF FCDR and the last block the CSU FCDR.

	F16	F17	F18
Bias [K]	-0.07	-0.03	+0.04
RSD [K]	0.40	0.35	0.36
MAD [K]	0.27	0.24	0.25
max absolute inter-sensor Bias [K]	0.11	0.07	0.11
Bias [K]	0.01	-0.02	0.00
RSD [K]	0.36	0.33	0.35
MAD [K]	0.24	0.23	0.23
max absolute inter-sensor Bias [K]	0.03	0.03	0.02
Trend [K/dec]	0.05 ($\alpha > 30\%$)	-0.10 ($\alpha > 30\%$)	0.09 ($\alpha > 30\%$)
Bias [K]	-0.02	-0.09	0.09
RSD [K]	0.36	0.34	0.34
MAD [K]	0.24	0.24	0.24
max absolute inter-sensor Bias [K]	0.11	0.18	0.18

Table III-4: Statistics of instrument differences for SSMIS channel 19v GHz. The numbers represent percentiles of absolute differences less than 1K, 2K, and 3K of all monthly mean grid boxes between two instruments.

	F16			F17			F18		
F13	78.7	95.1	98.6	72.6	92.2	97.5			
F14	76.3	94.3	98.4	71.8	91.4	97.1			
F16				84.2	97.1	99.4	83.9	97.3	99.5
F17							85.4	97.6	99.5

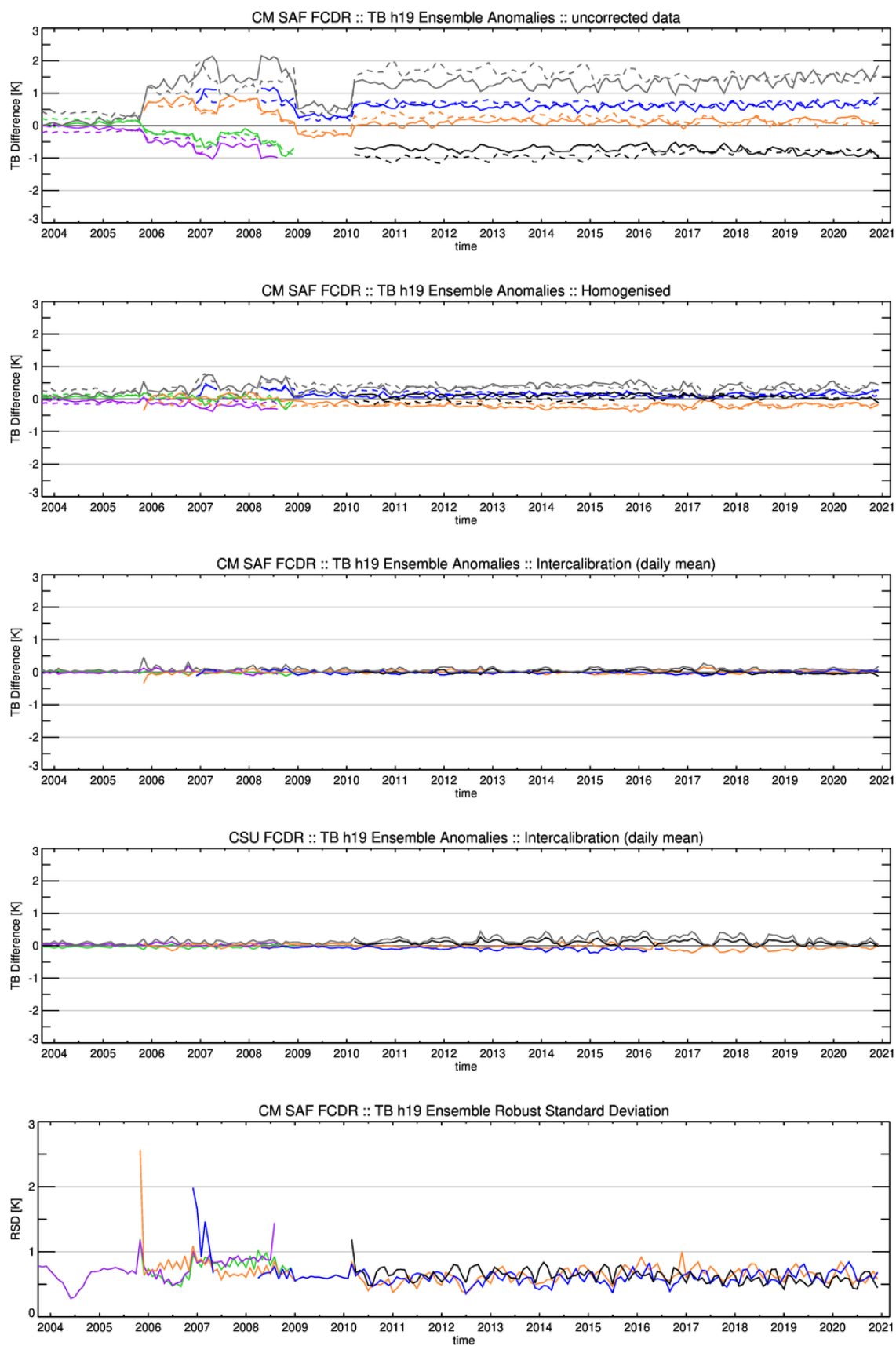


Figure III-7: Same as Figure III-6, but for SSM/I & SSMIS channel 19h GHz

Table III-5: Statistics of the ensemble anomalies for SSMIS channel 19h GHz. The first block shows the original RDR with EIA normalized, the second block the CM SAF FCDR and the last block the CSU FCDR.

	F16	F17	F18
Bias [K]	-0.16	+0.16	+0.04
RSD [K]	0.65	0.61	0.62
MAD [K]	0.46	0.43	0.43
max absolute inter-sensor Bias [K]	0.32	0.32	0.20
Bias [K]	+0.01	-0.01	0.00
RSD [K]	0.65	0.61	0.62
MAD [K]	0.44	0.41	0.42
max absolute inter-sensor Bias [K]	0.02	0.02	0.01
Trend [K/dec]	+0.01 ($\alpha > 30\%$)	+0.02 ($\alpha > 30\%$)	-0.04 ($\alpha > 30\%$)
Bias [K]	-0.03	-0.08	+0.10
RSD [K]	0.62	0.60	0.62
MAD [K]	0.42	0.41	0.42
max absolute inter-sensor Bias [K]	0.13	0.18	0.18

Table III-6: Statistics of instrument differences for SSMIS channel 19h GHz. The numbers represent percentiles of absolute differences less than 1K, 2K, and 3K of all monthly mean grid boxes between two instruments.

	F16			F17			F18		
F13	56.9	82.0	92.0	50.7	76.2	88.1			
F14	53.8	79.8	90.8	48.6	74.4	86.8			
F16				62.9	86.7	94.8	61.8	86.5	94.9
F17							64.1	87.7	95.5

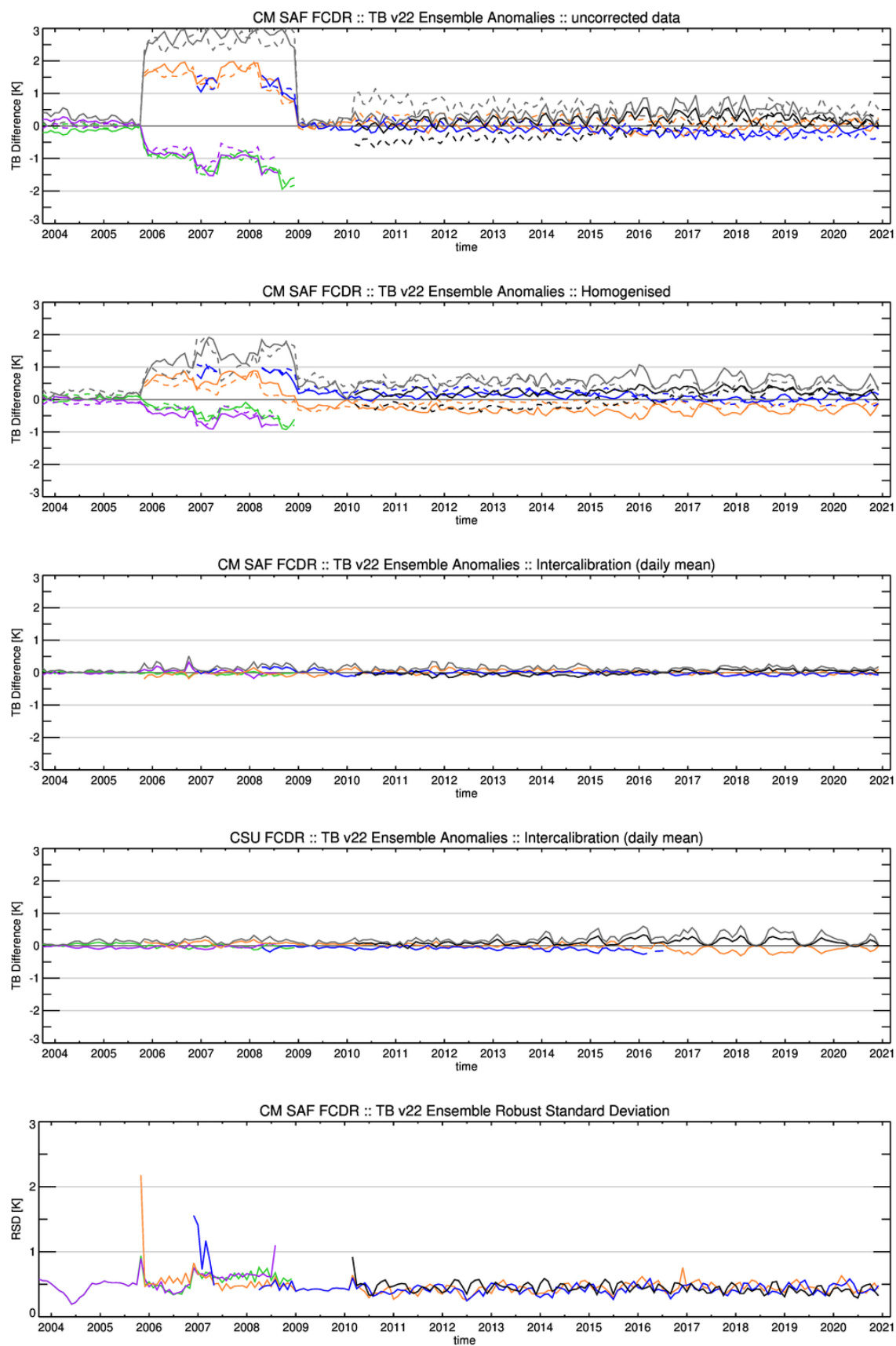


Figure III-8: Same as Figure III-6, but for SSM/I & SSMIS channel 22v GHz.

Table III-7: Statistics of the ensemble anomalies for SSMIS channel 22v GHz. The first block shows the original RDR with EIA normalized, the second block the CM SAF FCDR and the last block the CSU FCDR.

	F16	F17	F18
Bias [K]	-0.14	+0.18	+0.11
RSD [K]	0.55	0.49	0.47
MAD [K]	0.40	0.36	0.34
max absolute inter-sensor Bias [K]	0.32	0.32	0.25
Bias [K]	+0.01	-0.01	0.00
RSD [K]	0.46	0.44	0.44
MAD [K]	0.31	0.30	0.30
max absolute inter-sensor Bias [K]	0.02	0.02	0.01
Trend [K/dec]	+0.01 ($\alpha > 30\%$)	-0.07 ($\alpha > 30\%$)	+0.13 ($\alpha > 5\%$)
Bias [K]	-0.02	-0.08	+0.11
RSD [K]	0.46	0.44	0.45
MAD [K]	0.31	0.30	0.32
max absolute inter-sensor Bias [K]	0.13	0.19	0.19

Table III-8: Statistics of instrument differences for SSMIS channel 22v GHz. The numbers represent percentiles of absolute differences less than 1K, 2K, and 3K of all monthly mean grid boxes between two instruments.

	F16			F17			F18		
F13	69.1	90.3	96.4	60.8	84.4	93.2			
F14	66.8	89.3	96.0	58.3	82.7	92.3			
F16				76.4	94.2	98.2	76.2	94.5	98.5
F17							77.6	94.9	98.6

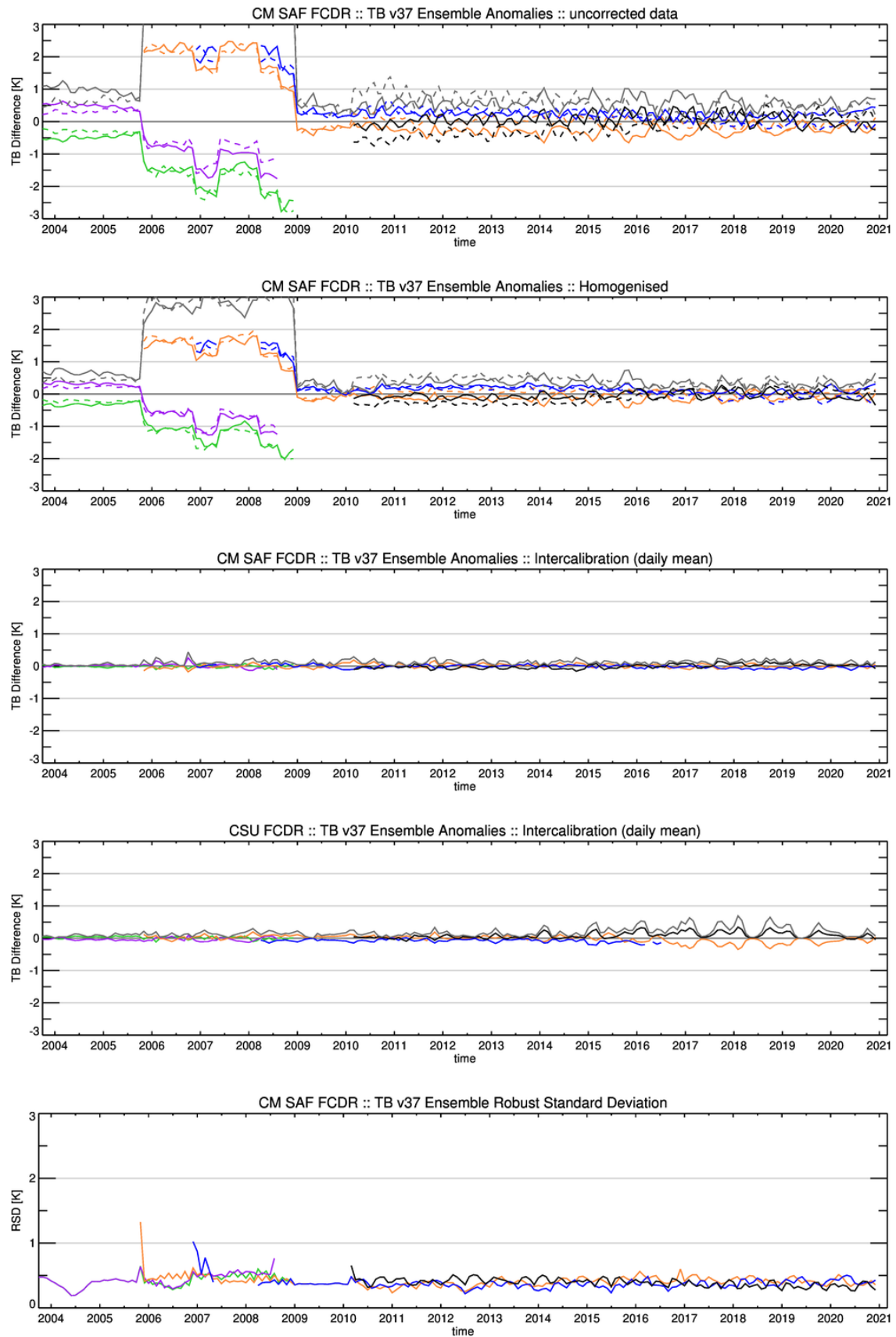


Figure III-9: Same as Figure III-6, but for SSM/I & SSMIS channel 37v GHz.

Table III-9: Statistics of the ensemble anomalies for SSMIS channel 37v GHz. The first block shows the original RDR with EIA normalized, the second block the CM SAF FCDR and the last block the CSU FCDR.

	F16	F17	F18
Bias [K]	+0.09	+0.15	-0.07
RSD [K]	0.57	0.44	0.42
MAD [K]	0.37	0.31	0.29
max absolute inter-sensor Bias [K]	0.16	0.22	0.22
Bias [K]	+0.01	-0.01	0.00
RSD [K]	0.41	0.38	0.39
MAD [K]	0.28	0.26	0.27
max absolute inter-sensor Bias [K]	0.02	0.02	0.01
Trend [K/dec]	+0.01 ($\alpha > 30\%$)	-0.06 ($\alpha > 30\%$)	+0.09 ($\alpha > 30\%$)
Bias [K]	-0.02	-0.08	+0.09
RSD [K]	0.40	0.37	0.40
MAD [K]	0.27	0.26	0.29
max absolute inter-sensor Bias [K]	0.11	0.17	0.17

Table III-10: Statistics of instrument differences for SSMIS channel 37v GHz. The numbers represent percentiles of absolute differences less than 1K, 2K, and 3K of all monthly mean grid boxes between two instruments.

	F16			F17			F18		
F13	76.4	94.7	98.6	72.0	92.4	97.7			
F14	73.2	93.5	98.2	71.0	91.6	97.3			
F16				81.1	96.7	99.3	80.1	96.7	99.4
F17							82.6	97.2	99.5

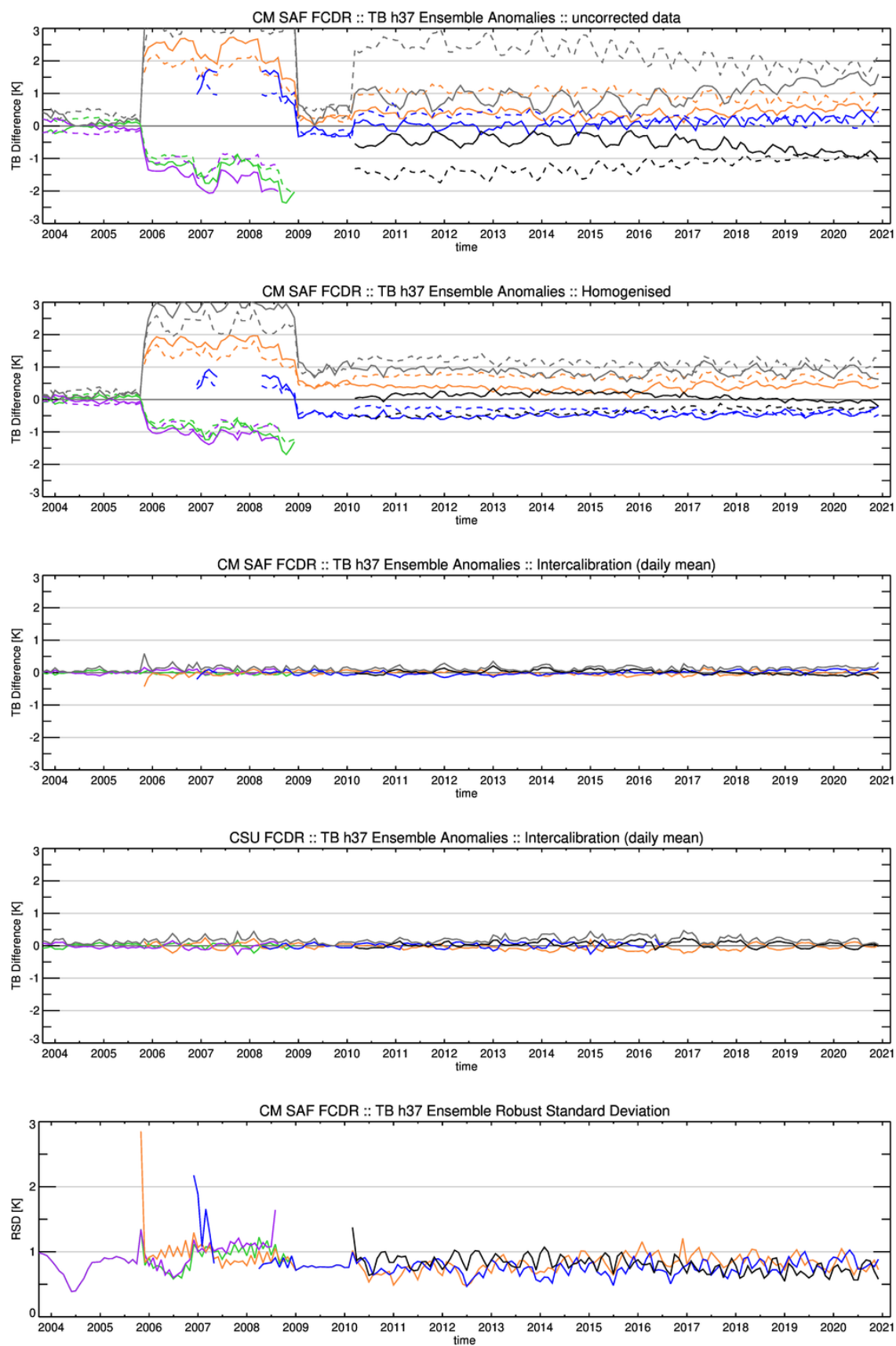


Figure III-10: Same as Figure III-6, but for SSM/I & SSMIS channel 37h GHz.

Table III-11: Statistics of the ensemble anomalies for SSMIS channel 37h GHz. The first block shows the original RDR with EIA normalized, the second block the CM SAF FCDR and the last block the CSU FCDR.

	F16	F17	F18
Bias [K]	+0.69	-0.36	-0.13
RSD [K]	0.94	0.81	0.81
MAD [K]	0.83	0.64	0.55
max absolute inter-sensor Bias [K]	1.05	1.05	0.82
Bias [K]	-0.01	-0.01	+0.01
RSD [K]	0.83	0.77	0.80
MAD [K]	0.56	0.52	0.54
max absolute inter-sensor Bias [K]	0.02	0.02	0.02
Trend [K/dec]	0.00 ($\alpha > 30\%$)	+0.09 ($\alpha > 30\%$)	-0.12 ($\alpha > 30\%$)
Bias [K]	-0.03	+0.01	+0.04
RSD [K]	0.80	0.82	0.80
MAD [K]	0.54	0.55	0.54
max absolute inter-sensor Bias [K]	0.07	0.04	0.07

Table III-12: Statistics of instrument differences for SSMIS channel 37h GHz. The numbers represent percentiles of absolute differences less than 1K, 2K, and 3K of all monthly mean grid boxes between two instruments.

	F16			F17			F18		
F13	48.3	75.6	88.4	44.1	70.8	84.7			
F14	44.9	72.4	86.3	42.8	69.4	83.6			
F16				53.5	80.4	91.7	51.7	79.4	91.5
F17							54.7	81.8	92.7

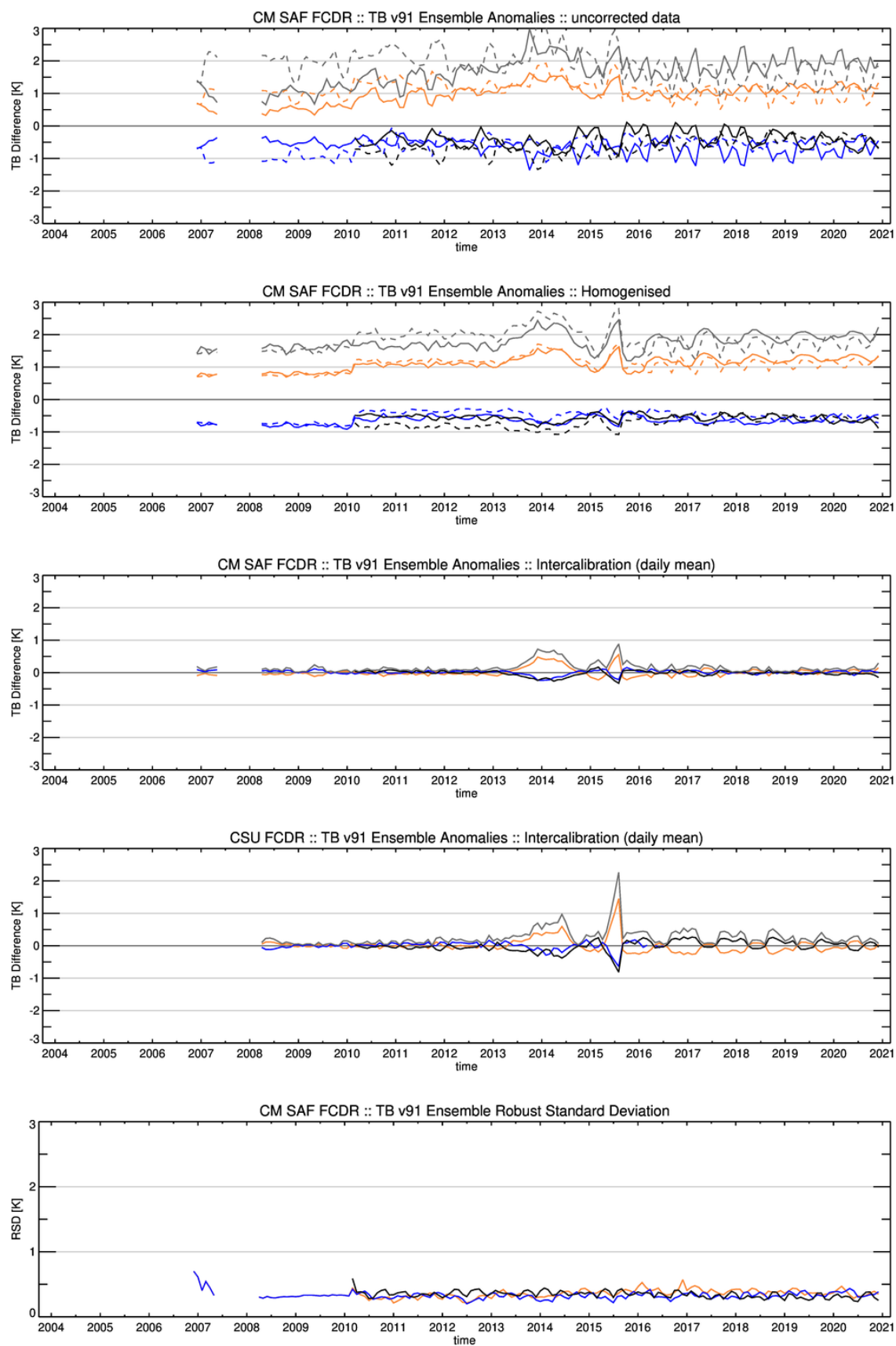


Figure III-11: Same as Figure III-6, but for SSMIS channel 91v GHz.

Table III-13: Statistics of the ensemble anomalies for SSMIS channel 91v GHz. The first block shows the original RDR with EIA normalized, the second block the CM SAF FCDR and the last block the CSU FCDR.

	F16	F17	F18
Bias [K]	+1.11	-0.58	-0.64
RSD [K]	0.43	0.37	0.59
MAD [K]	1.1	0.59	0.64
max absolute inter-sensor Bias [K]	1.75	1.69	1.75
Bias [K]	+0.00	0.01	-0.02
RSD [K]	0.38	0.34	0.35
MAD [K]	0.26	0.23	0.24
max absolute inter-sensor Bias [K]	0.02	0.03	0.03
Trend [K/dec]	+0.06 ($\alpha > 30\%$)	-0.01 ($\alpha > 30\%$)	-0.06 ($\alpha > 30\%$)
Bias [K]	-0.01	0.00	0.00
RSD [K]	0.38	0.36	0.40
MAD [K]	0.26	0.24	0.27
max absolute inter-sensor Bias [K]	0.01	0.01	0.01

Table III-14: Statistics of instrument differences for SSMIS channel 91v GHz. The numbers represent percentiles of absolute differences less than 1K, 2K, and 3K of all monthly mean grid boxes between two instruments.

	F16	F17	F18
F16		84.6 98.2 99.7	83.6 98.2 99.8
F17			87.9 98.8 99.9

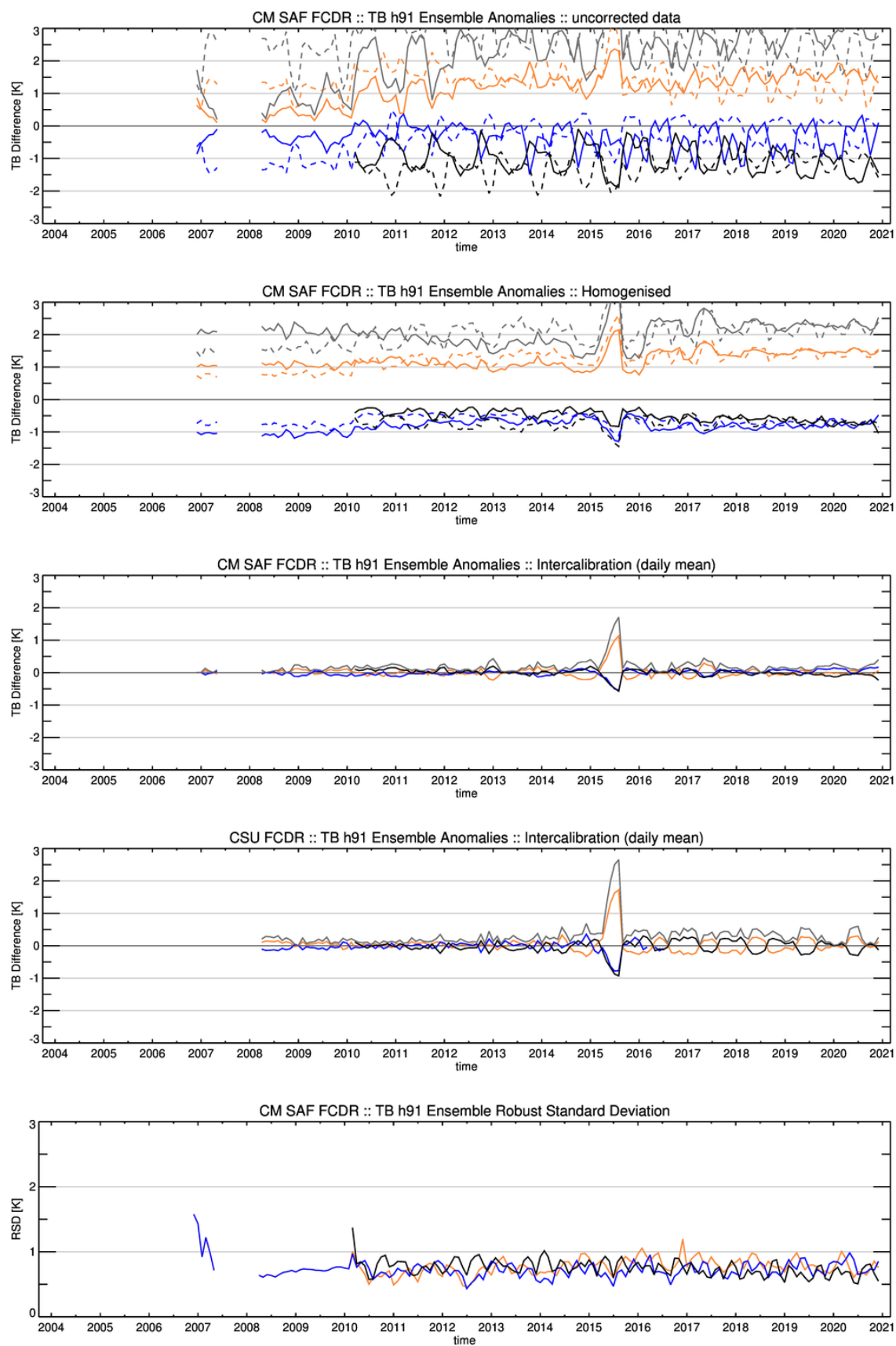


Figure III-12: Same as Figure III-6, but for SSMIS channel 91h GHz.

Table III-15: Statistics of the ensemble anomalies for SSMIS channel 91h GHz. The first block shows the original RDR with EIA normalized, the second block the CM SAF FCDR and the last block the CSU FCDR.

	F16	F17	F18
Bias [K]	+1.22	-0.73	-0.61
RSD [K]	0.86	0.76	0.77
MAD [K]	1.25	0.81	0.74
max absolute inter-sensor Bias [K]	1.95	1.95	1.83
Bias [K]	+0.01	-0.01	0.00
RSD [K]	0.78	0.73	0.75
MAD [K]	0.52	0.49	0.51
max absolute inter-sensor Bias [K]	0.02	0.02	0.01
Trend [K/dec]	-0.03 ($\alpha > 30\%$)	0.12 ($\alpha > 30\%$)	-0.14 ($\alpha > 5\%$)
Bias [K]	+0.03	-0.03	-0.02
RSD [K]	0.75	0.74	0.78
MAD [K]	0.51	0.50	0.53
max absolute inter-sensor Bias [K]	0.06	0.06	0.05

Table III-16: Statistics of instrument differences for SSMIS channel 91h GHz. The numbers represent percentiles of absolute differences less than 1K, 2K, and 3K of all monthly mean grid boxes between two instruments.

	F16	F17	F18
F16		54.7 82.5 93.5	53.7 82.0 93.5
F17			57.4 84.8 94.9

III-5 Comparison against GMI

Another type of evaluation of the SSMIS FCDR is to analyse the brightness temperatures relative to another independent, stable observation. This option became possible with the availability of data from the GPM Microwave Imager (GMI). The Global Precipitation Measurement (GPM) platform was launched end of February 2014. The platform is in a non-synchronous orbit, with an inclination of 65 degrees. This type of orbit allows a sampling of all local Earth times in about two weeks, covering the Earth within about ± 70 degree latitude.

The GMI is a dual-polarization, conical-scanning, passive microwave radiometer. The principle design of the instrument and the strict calibration accuracy enables it to serve as a high-quality in-orbit reference instrument. More information about the GMI instrument is given by Draper et al. (2015).

The GMI centre frequencies are shifted relative to the SSMIS frequencies. The SSMIS-like channels are centred at 18.7, 23.8, 36.5 and 89.0 GHz and are sampled at horizontal and vertical polarization, except the 23.8 GHz channel. GMI level-1 data records are available at the NASA PPS data server (<https://arthurhou.pps.eosdis.nasa.gov/>). Due to the shift in the channel frequencies, an absolute difference between the observations from GMI and SSMIS is expected. However, all SSMIS instruments should depict the same difference after all calibration offsets are applied.

The comparison against GMI is done, similar to the inter-sensor evaluation, for monthly mean values. The instantaneous observations from all instruments are gridded into daily global 1° equal angle grids. As the GMI is in a non-synchronous orbit, ascending and descending orbits are directly compiled into daily mean gridded fields for each channel. The monthly mean anomalies between the SSMIS T_B and the GMI $T_{B,GMI}$ are then calculated for each grid cell. Following the notation established in section III-4.3, the brightness temperature anomalies at each grid point g , time step t and instruments s are then defined as:

$$\Delta T_B(s, t, g) = T_B(s, t, g) - T_{B,GMI}(t, g). \quad \text{Equation 6}$$

In order to compare the characteristics of the time series for both instruments, the global median $\overline{\Delta T_{B,s}}(t)$ is derived for each month. The time series' of these anomalies are presented in Figure III-13 to Figure III-16. All figure panels contain two images for each frequency and polarisation with the global monthly mean values of:

1. T_B anomalies with reflector emissivity correction and EIA normalization applied,
2. T_B anomalies of the CM SAF FCDR with inter-sensor calibration offsets and solar calibration correction offsets applied.

As expected, the final differences can be quite large due to the differences in the centre frequency of the compared channels, which is not adjusted. The largest differences are found for the 19.35 GHz (18.7 GHz) channels with about 6 K and 9 K.

However, after the application of the inter-sensor correction offsets to the SSMIS brightness temperatures, the observed differences between the three sensors are removed and no significant trend can be observed.

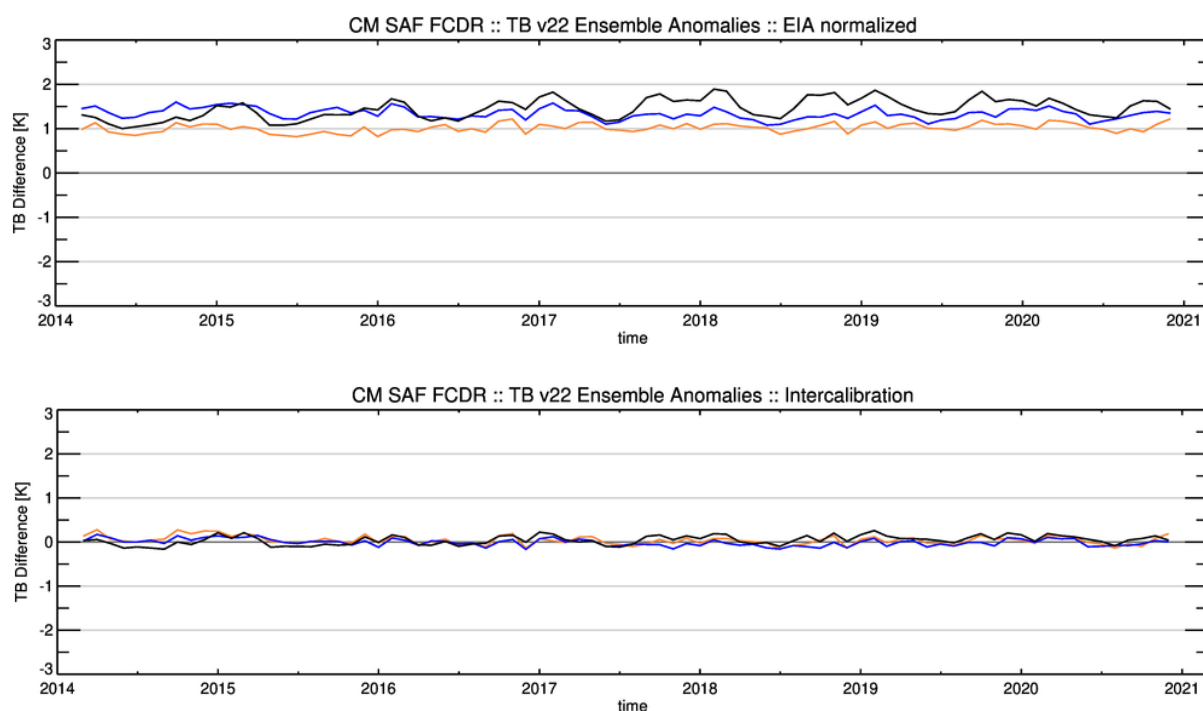


Figure III-13: Time series of global monthly mean anomalies of SSMIS minus GMI brightness temperatures at 22 GHz. The upper panel shows the homogenised data records and the lower panel depicts the inter-sensor calibrated SSMIS data record. Colours are as in Figure III-1.

A regular seasonal signal is visible for the uncorrected the SSMIS_{F18} data, most pronounced in the 22v and the 37v channels. This feature also corresponds to a seasonal variation found in the inter-sensor validation (see section III-4.4). However, by comparing to an independent data record, it becomes clear that this variation is mainly caused by the SSMIS_{F18}. The newly developed solar calibration correction removes this issue. Also, the previously identified anomalies in the 91 GHz are clearly visible in 2014 and 2015.

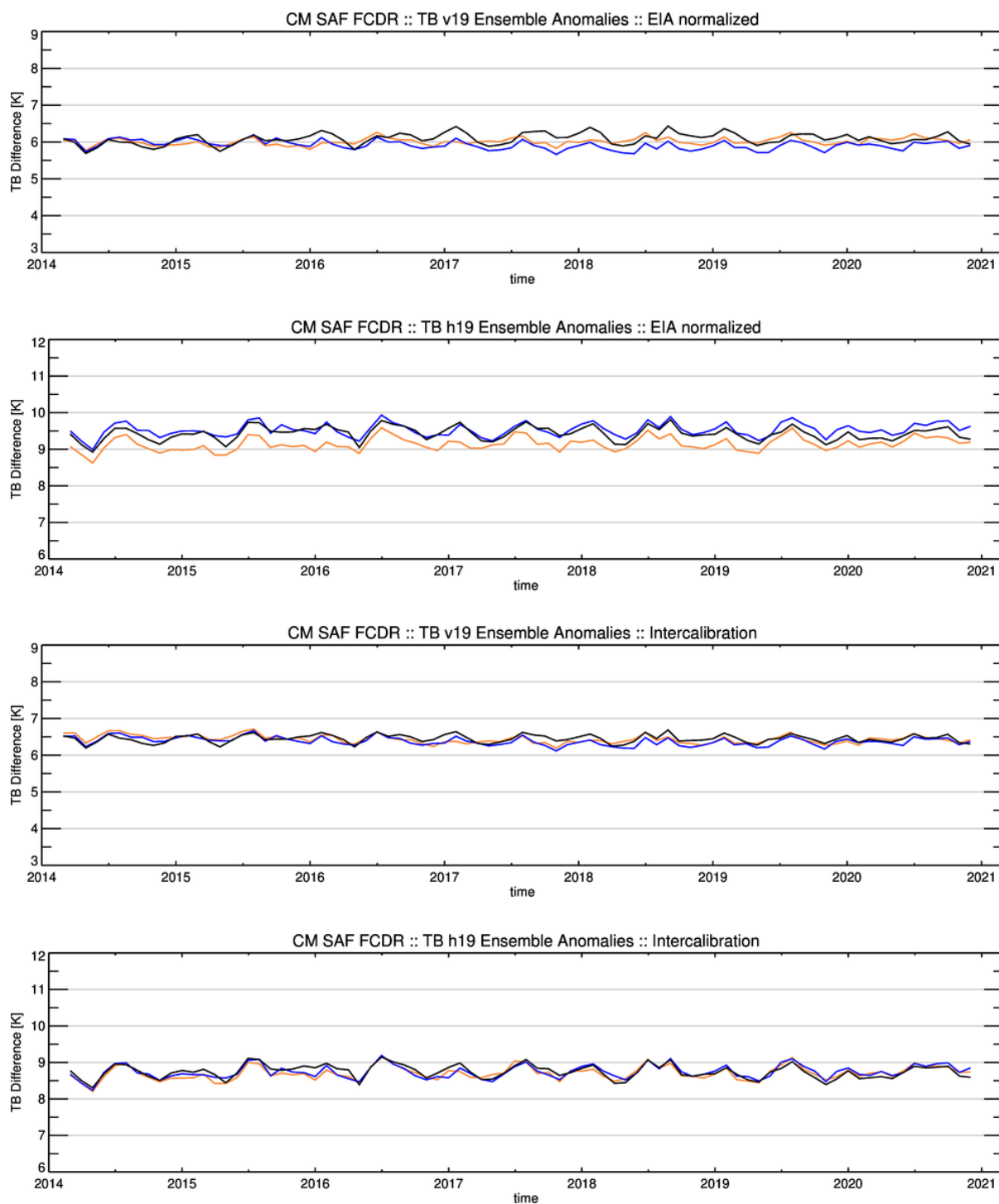


Figure III-14: Time series of global monthly mean anomalies of SSMIS minus GMI brightness temperatures at 19 GHz. The upper two panels show the homogenised data records and the two lower panels depict the inter-sensor calibrated SSMIS data record. Colours are as in Figure III-1.

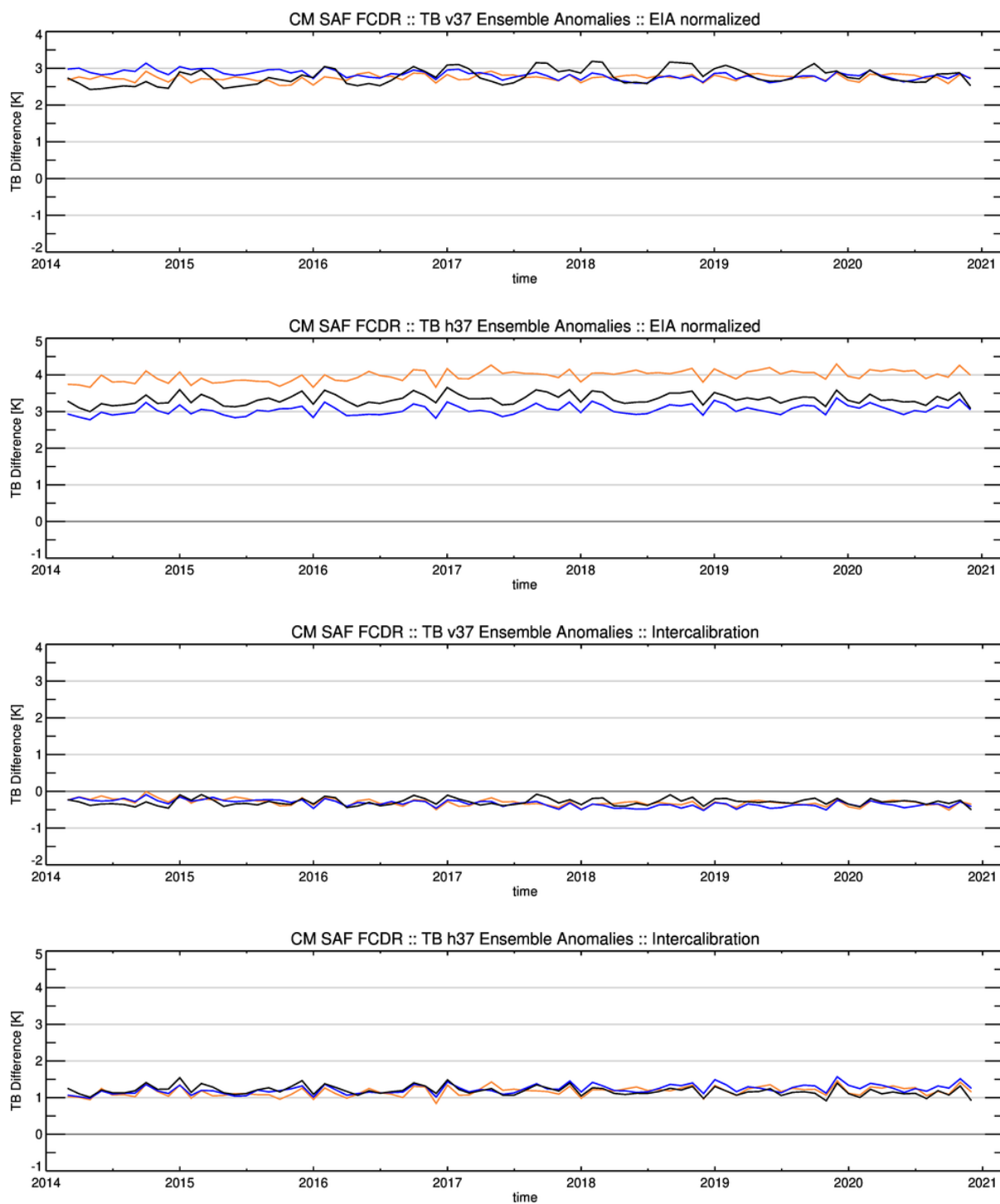


Figure III-15: Time series of global monthly mean anomalies and SSMIS minus GMI channels at 37 GHz. The upper two panels show the homogenised data records and the two lower panels depict the inter-sensor calibrated SSMIS data record. Colours are as in Figure III-1.

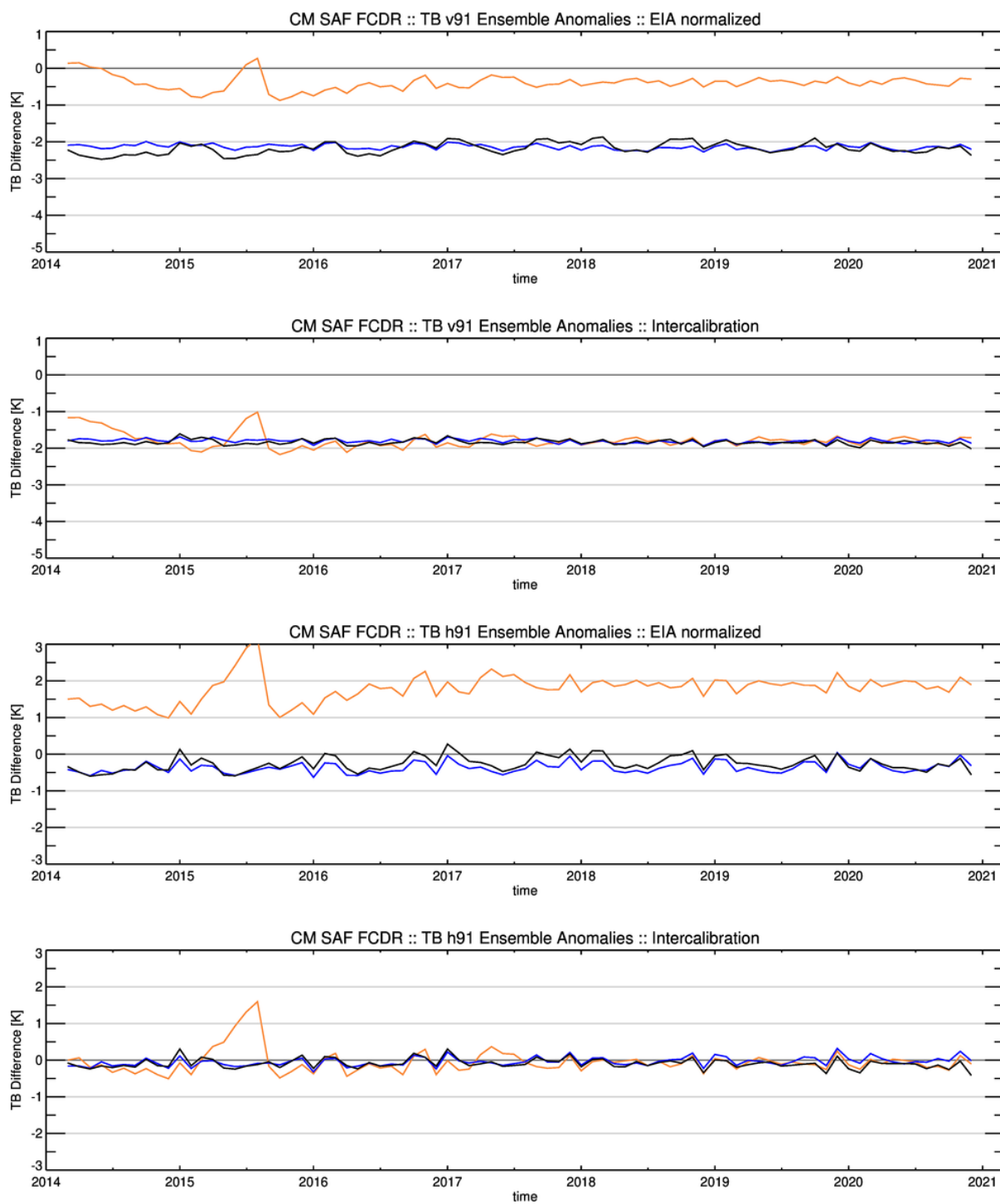


Figure III-16: Time series of global monthly mean anomalies and SSMIS minus GMI channels at 91 GHz. The upper two panels show the homogenised data records and the two lower panels depict the inter-sensor calibrated SSMIS data record. Colours are as in Figure III-1.

IV SMMR

The CM SAF FCDR from SMMR brightness temperatures consists of daily collections of all observations. All sensor specific data available in the input Level 1B data records are provided, as well as additional information like quality control flags and inter-sensor calibration offsets. The SMMR FCDR is available for the time period from October 1978 until August 1987.

A technical description of the data set, including information on the file format as well as on the data access is provided in the corresponding Product User Manual [RD 6]. Furthermore details on the CM SAF inter-sensor calibration model, the implementation of the processing chain and individual processing steps are described in the SMMR Algorithm Theoretical Basis Document [RD 7].

IV-1 Instrument and sensor stability

Figure IV-1 shows the time series of Nimbus-7 local equator crossing time (a), data coverage (b), platform altitude (c), platform attitude angles (d), and Earth incidence angles (e). In contrast to the DMSP platforms, the Nimbus-7 equator crossing time remains quite constant at 12 AM/PM throughout the lifetime. Just a small drift can be observed during the last two years in operation. The SMMR data coverage is quite constant at a level of about 50 %, keeping in mind that the SMMR operated on a 50 % duty cycle for most of the time. During the special operations period from April to June 1986, the coverage is reduced to just about 20%. In the first few months nearly 90 % coverage was achieved.

The platform altitude (Figure IV-1, panel c) depicts a short increase during the first months in operation but remains constant thereafter. The mean platform attitude roll and yaw angles (Figure IV-1, panel d) are also inconspicuous. However, the pitch angle depicts a sharp drop in January 1984 to -0.4° and then a second smaller step in September 1984 to -0.5° . Also the seasonal variability increased with this second step. This behaviour was noted already by Francis (1987). The main impact of a change in the pitch angle is on the EIA (Figure IV-1, panel e). The mean EIA changed by about 0.7° from around 50.3° before 1984 to 49.6° after September 1984. Due to this change, the mean vertically polarised brightness temperatures changed by about 1 K. Therefore, it has to be kept in mind to always account for true EIAs when using the SMMR TBs.

Figure IV-2 (a) shows the time series of various instrument temperature readings (engineering data) exemplarily for the 18h channel. The engineering data for the other channels (not shown here) are similar to the presented 18h channel. The mean instrument temperatures remain constant at around 300 K throughout the lifetime of the instrument. The drop in 1986 is due to limited coverage in the special operations period, when the instrument was only operating at some parts of the orbit. In this case the observed mean values do not represent a global mean. A small periodic seasonal variation with 2 K peak to peak can be observed in the engineering data with a maximum in the winter season and a minimum in the summer season.

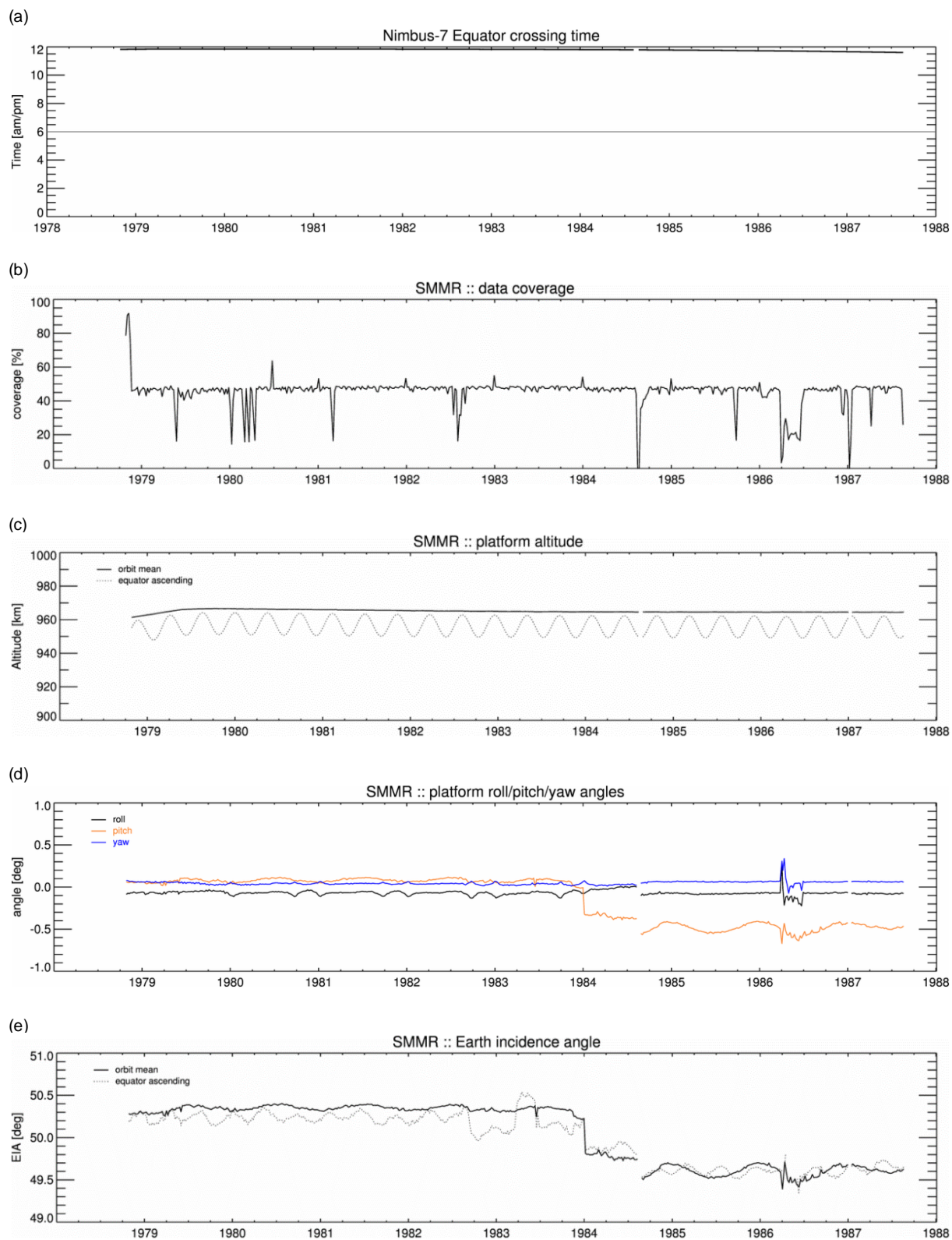


Figure IV-1: Time series of Nimbus-7 local equator crossing time (a), data coverage (b), platform altitude (c), platform attitude angles (d), and Earth incidence angles (e). Thin dotted lines are the mean values at the ascending equator crossing and thick lines depict complete orbit mean values.

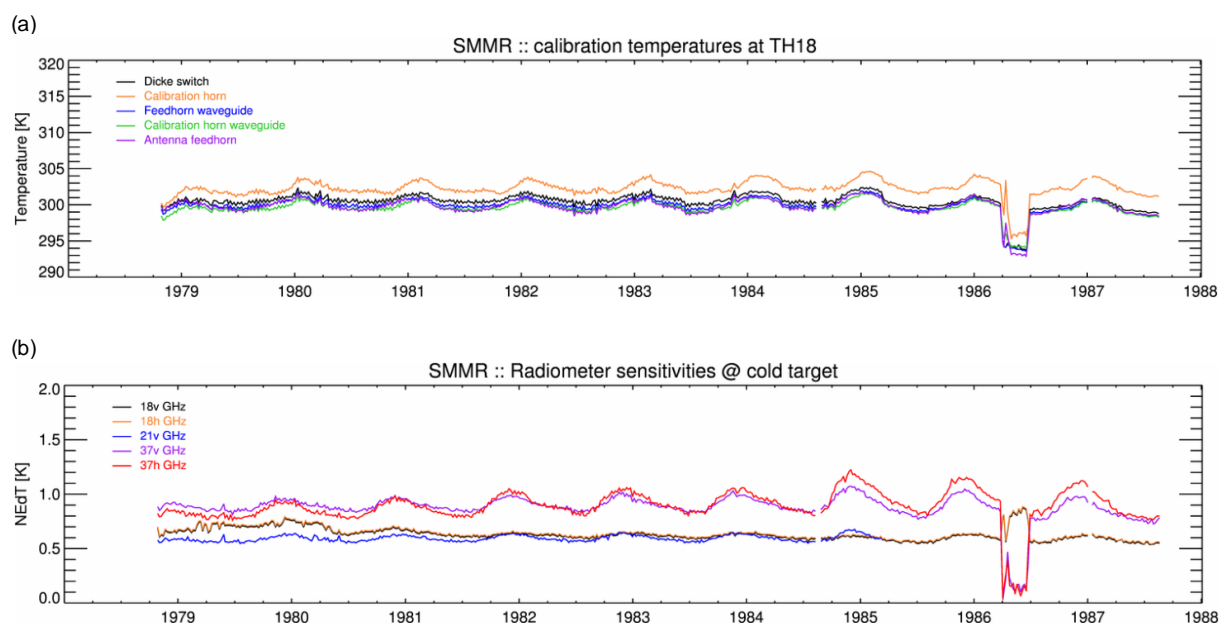


Figure IV-2: Time series of various instrument calibration temperature readings for the 18h channel (a) and radiometer sensitivities $NEdT$ (b) for the SSM/I like channels.

The time series of radiometer sensitivities ($NEdT$) at the cold calibration target for the SSM/I like channels is presented in Figure IV-2 (b). The mean values of the 21 and 37 GHz channels remain constant at approximately 0.6 K and 0.9 K, respectively. The mean $NEdT$ value of the 19 GHz channels drops slightly from 0.7 K to 0.6 K during 1981. All channels depict a periodic seasonal variation with maxima in the winter season. The largest peak to peak variations can be seen for the 37 GHz channels. For these channels the seasonal variation is increasing year by year from 0.8 K to about 1.1 K.

IV-2 Instrument evaluation

Conducting a direct inter-sensor validation for the SMMR, as it was done for the SSMI(S) instruments, is not feasible. The overlap time period is just a month and SMMR data is available only every other day. In case of the 21 GHz channel, there is no overlap at all as this failed in 1985. Also the channels are not at the exact same centre frequency (18 and 21 GHz instead of 19 and 22 GHz). Therefore, a common stable reference has to be used for both instruments and the anomaly against this reference needs to be analysed. Ideally one would select one reference for the inter-calibration and another one for the evaluation. Here it was decided to use ERA-20C (Poli et al., 2013), because it relies only on surface pressure and sea-ice information and does not assimilate satellite data. Thus, ERA-20C is independent from the FCDR and has a high potential to be stable.

In order to minimize the influence of diurnal cycle, unknown surface emissivities and scattering effects, the comparison was limited to only cloud-free and lightly cloudy scenes over water surfaces. Brightness temperatures at the top of the atmosphere are calculated for the filtered data record with RTTOV 11.2 (Saunders et al. 2013) and the surface emissivity with FASTEM 6 (Meunier et al. 2014). Profiles from ERA20C are available every 3 hours, resulting in maximum time differences of 90 minutes between observed and simulated brightness temperatures. The simulations are done for the entire time period covered by SMMR and

SSM/I aboard F08. In order to reduce the uncertainty in the observed differences, the match-up data is then gridded into daily global 1° equal angle grids, separately for ascending and descending orbits and these are combined to daily means.

The monthly mean anomalies between the observation T_B and the model T_{BM} are calculated for each grid cell. Following the notation established in section III-4.3, the anomalies at each grid point are then defined as:

$$\Delta T_B(s, t, g) = T_B(s, t, g) - T_{BM}(s, t, g). \quad \text{Equation 7}$$

In order to compare the characteristics of the time series for both instruments, global median ($\overline{\Delta T_{B,s}}(t)$) and robust standard deviation ($RSD_s(t)$) are derived for each month.

Figure IV-3 shows the global monthly mean anomaly time series of SMMR and SSM/I_{F08} before and after inter-calibration. The SSM/I_{F08} itself is inter-calibrated to the SSM/I aboard F11, which is the FCDR calibration reference instrument. This means the SSM/I_{F08} is used as a transfer target. The relative differences without inter-calibration range between -0.5 K and 5.3 K for the 37h and 37v GHz channel, respectively. Overall the SMMR anomalies depict a larger seasonal variation compared to the SSM/I for the 19 and the 22 GHz channel. After applying the inter-calibration, all mean relative difference are significantly reduced to below 0.1 K. The time series for the 37 GHz channels are stable and a good continuity to the F08 is apparent in Figure IV-3. The 21 GHz channel depicts an upward trend of about 1 K from 1984 until it failed. Also the 19 GHz channels are showing a step in 1984. This corresponds to the observed EIA change in 1984. This might also be an indication of unresolved issues with attitude of the platform or some shortcoming in the surface emissivity model at that zenith angle. Also the seasonal variability is significantly larger for the lower frequencies, compared to the SSM/I.

The anomalies are statistically analysed following the notations defined in section III-4.3. Mean bias and RSD after inter-calibration are summarized in Table IV-1. Recalling that 68 % of all data samples are within 1 standard deviation of a Gaussian distribution, the mean robust standard deviation is a statistical measure for all monthly mean 1° anomalies. However, it must also be accounted for the natural variability and uncertainties in the forward model and the reanalysis data. Therefore only the relative differences between SSM/I_{F08} and SMMR are important (given in the column labelled Delta), not the absolute values. The SSM/I_{F08} is inter-calibrated to the reference instrument on-board F11 and the reanalysis is only used as a transfer standard. Under these conditions, the horizontally polarized channels of the SMMR are similar to the SSM/I, but the vertically polarized channels show larger RSDs. Especially the 22v channel depicts a significantly larger noise. So it can be concluded, that the monthly mean inter-calibrated SMMR brightness temperatures are better than the target criterion. The estimated linear trends are not significant, given the large variability on the global monthly mean anomalies.

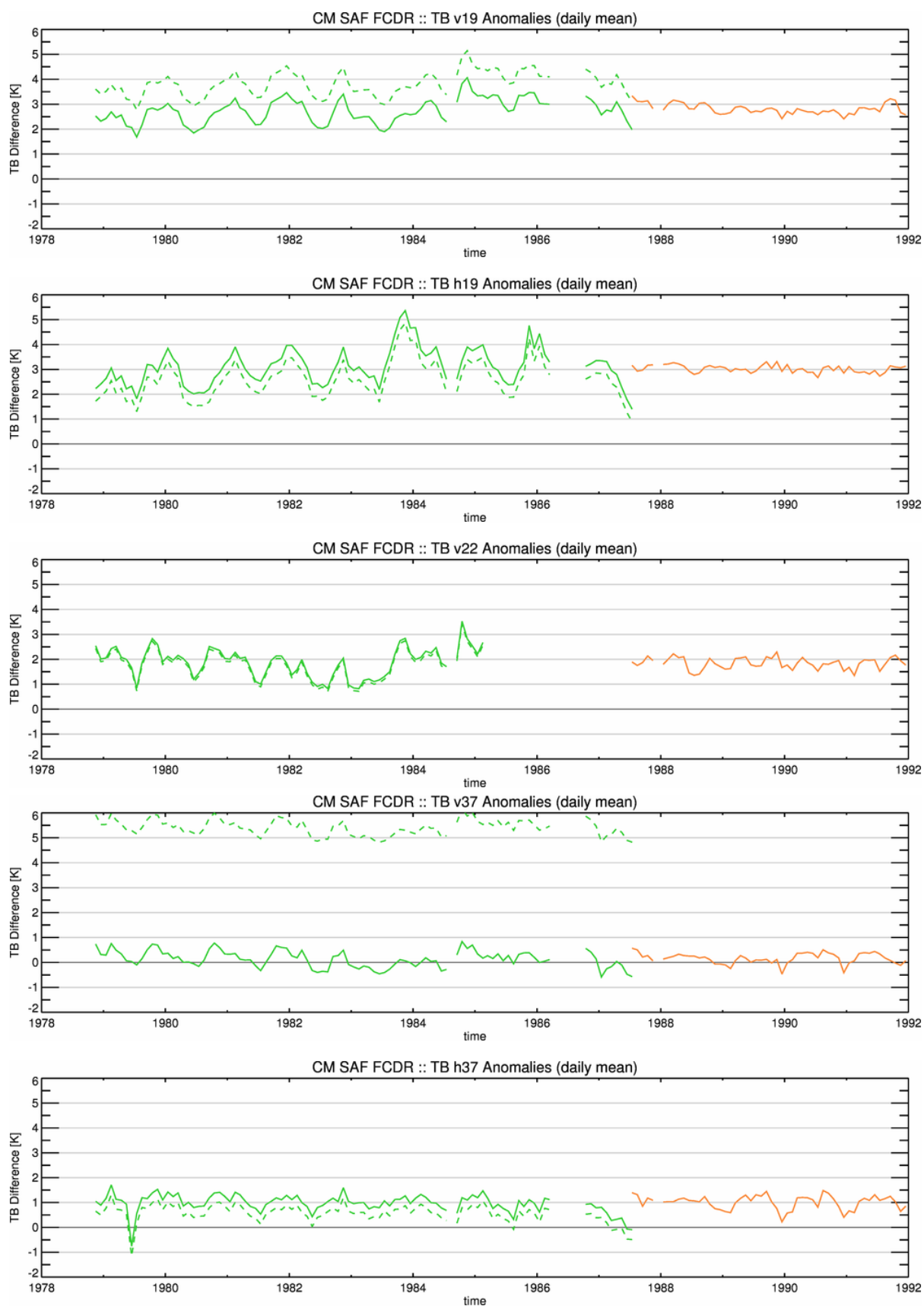


Figure IV-3: Time series of global monthly mean anomalies between observed and modelled TBs before (dashed lines) and after (solid lines) inter-calibration of SMMR for all FCDR channels. (SMMR, green; F08 orange).

Table IV-1: Statistics for the SMMR FCDR channel brightness temperature anomalies.

	Bias [K]			RSD [K]		
	SMMR	SSM/I F08	Delta	SMMR	SSM/I F08	Delta
18 / 19 GHz v	2.7	2.8	0.1	1.6	1.3	0.3
18 / 19 GHz h	3.0	3.0	0.0	2.2	2.1	0.1
21 / 22 GHz v	1.9	1.8	0.1	2.8	2.2	0.6
37 GHz v	0.2	0.2	0.0	1.6	1.3	0.3
37 GHz h	1.0	1.0	0.0	2.7	2.8	0.1

V Evaluation of brightness temperature differences against reanalysis

Additionally, to the inter-sensor comparison in section III-4, a more complete analysis of each individual channel across the sensors for the complete time period was conducted. The idea is to derive an improved characterisation of the long-term FCDR stability, using independent reanalysis data records. However, this approach is hampered due to several constraints. The basic assumptions are that the reanalysis is independent of the observations, stable in time and does cover the complete time period of the FCDR. Moreover, the uncertainties in the applied radiative transfer model and the surface emissivity model should be well behaved and characterised. However, there is actually no reanalyses available fulfilling all the constraints.

The first choice to evaluate the FCDR is to use the ERA-20C reanalysis similar to the SMMR inter-calibration and evaluation, as it does not assimilate any satellite observations, being independent from the FCDR. However, the covered time period ends already in 2010. This does not allow a complete analysis of the transition from SSM/I to SSMIS with SSMIS_{F18} data becoming available in 2010. Therefore, also the ERA5 reanalysis (Hersbach et al., 2020) was used in the evaluation process, although it does not fulfil our requirements. Firstly, it is not independent as it assimilates SSM/I and SSMIS data records. Moreover, the SSM/I part of this CM SAF FCDR is assimilated. Secondly, it is also not stable in time, as the composition of the assimilated observation systems is changing over time.

A serious limitation in the comparison is the large uncertainty of surface emissivity models over land, sea-ice and snow covered surfaces due to unknown surface emissivities. Also, the strong diurnal cycle over land is likely not fully resolved by the reanalysis. Additionally, rainy and cloudy scenes increase the uncertainty of the radiative transfer model due to scattering effects of the water droplets. In order to minimize these influences, only cloud-free and lightly cloudy scenes over water surfaces are selected for the match-up data sets. However, this practically limits this comparison to the cold end of the natural spectrum and no conclusion can be drawn for the scene dependence or the warm end of the spectrum.

Brightness temperatures at the top of the atmosphere are calculated for the filtered data record with RTTOV 11.2 (Saunders et al. 2013) and the surface emissivity with FASTEM 6 (Meunier et al. 2014). Profiles from ERA-20C are available every 3 hours, resulting in maximum time differences of 90 minutes between observed and simulated brightness temperatures. Profiles from ERA5 are available every hour. However, in order to limit the overall data volume, the same temporal sampling of 3 hours like for ERA-20C is selected. The simulations are done for the entire time period covered by the FCDR. In order to reduce the uncertainty in the observed differences, the match-up data is then gridded into daily global 1° equal angle grids, separately for ascending and descending orbits.

The monthly mean anomalies between the observation T_B and the model T_{BM} are calculated for each grid cell. Following the notation in section IV-2 the anomalies at each grid point are then defined as in Equation 7. In order to compare the characteristics of the time series for all instruments and both reanalysis, global median $(\overline{\Delta T_{B,s}}(t))$ and robust standard deviation $(RSD_s(t))$ are derived for each month.

V-7 Evaluation results

The time series for AM/PM global monthly mean anomalies are shown for all FCDR channels in Figure V-2 to Figure V-9 and the robust standard deviations (RSD) for the vertically polarised channels in Figure V-10 for ERA-20C and in Figure V-11 for ERA5. The RSD for the horizontally polarized channels are not shown here, as the trends are very similar to the vertically polarised channels. All mean figure panels contain four images with global monthly mean time series of:

1. anomalies between raw data records (with reflector emissivity correction, intrusion correction, and EIA normalisation applied) and ERA-20C,
2. anomalies between inter-calibrated data records (all corrections applied) and ERA-20C,
3. anomalies between raw data records (with reflector emissivity correction, intrusion correction applied, and EIA normalisation applied) and ERA5,
4. anomalies between inter-calibrated data records (all corrections applied) and ERA5.

The general conclusions from these comparisons are very similar to the results from the inter-sensor comparisons. The largest inter-sensor differences are observed at the higher frequencies (37 GHz and 85 GHz) with values in the order of 3 to 4 K. Maximum differences are found for the channel 37v between the SSMR and SSM/I_{F08} of more than 6 K. Best agreement between the sensors is found for the 19 GHz v-pol channel, with values below 1 K.

The applied inter-calibration effectively removes the observed differences. The residual TB inter-satellite difference is in the order of 0.1 to 0.2 K after applying the inter-sensor calibration for most of the channels and instrument combinations. The final differences stay within 1 K over the whole time-period. The largest remaining deviations are found for the synthetic 85 GHz channels. These are used when the 85 GHz channels failed on F08 (after December 1987) and for the SSMIS, where the corresponding channel is at 91 GHz.

The mean residuals at 85 GHz for the transition from SSM/I_{F08} to SSM/I_{F10} are around 0.5 K. The original differences for the transition from SSM/I to SSMIS are around 0.6 K for the channel 85v and 0.8 K for the channel 85h. However, these offsets are much smaller, when only inter-satellite differences are analysed (not shown). Further investigations showed, that this is related to the different filtering of the analysed data. While for the forward calculations only cloud-free and lightly cloudy scenes are used, the full spectrum of brightness temperatures is used for the inter-sensor evaluation. The main reasons for the observed differences are a scene depending non-linear residual over ocean and an ascending/descending bias of the SSMIS_{F16}, 91 GHz channels during the overlap period with SSM/I_{F13}. In order to minimize the inhomogeneity of the time-series, an additional correction was derived (see [RD 1]) and the more stable ascending orbits are used as inter-calibration reference. The depicted plots in Figure V-6 and Figure V-7 are with the additional correction applied. The final differences are now in the order of 0.1 K.

Another prominent feature is the application of a relative inter-calibration to the reference instrument aboard F11. It is not possible to see this in the inter-satellite comparison as only relative differences are analysed. From the model based evaluation it becomes clear, that any

offset in the SSM/I_{F11} is transferred to the other instruments. This might not always be the optimum, but leads to homogenous time series with all instruments acting as a synthetic F11.

The mean anomalies are very similar for ERA-20c and ERA5. Conclusions concerning the temporal stability are difficult to derive, because the variations can be caused by the FCDR or the reanalysis. Overall, most channels depict a negative decadal trend in the order of -0.1 K/decade. This decrease starts in the early 1990s and persists until around 2009, when the SSM/I covered era ends. The strongest decrease can be observed in the 85 GHz channels. From 2010 onwards, the anomaly time series of all channels are very stable. However, this behaviour is very consistent for all channels as the FCDR instruments overlap and follow each other very close. It is unlikely, that a degradation of the quality occurs in all channels of all instruments. A hypothesis would be, that this trend is caused by the density of assimilated data improving over time.

The anomalies from ERA-20C exhibit a larger month-to-month variability. This also becomes clear from the RSD values (see Figure V-10 and Figure V-11), which are significantly larger than the ERA5 values. A small decrease in the RSD of the 22 GHz and 85 GHz channels can be observed for ERA-20c. As all FCDR instruments do depict the same trend, it is assumed to be caused by changes in ERA-20C, possibly due to an improvement in the density of assimilated data. The RSD values of ERA5 are very constant over time, only SMMR and SSM/I_{F08} depict higher values.

In order to perform a linear trend analysis for the complete SSM/I and SSMIS period, all individual instrument anomalies are averaged to provide a single data record for a specific frequency. The long-term trend is then estimated using Equation 5 with these mean anomalies and summarized in Table V-1. The trend for 91 GHz is not given for ERA-20c, because the time period is too short to estimate a meaningful value. The derived trends are very similar for ERA-20c and ERA5, with the maximum of -0.17 K/decade for the 37 GHz channel in ERA-20c. This is still about the same order as the standard deviation of the global mean time series. The

Table V-1: Estimated trends for global monthly mean differences between the simulated brightness temperatures from ERA-20c and ERA5 and the combined inter-calibrated FCDR.

Channel	Trend ERA-20c [K/dec]		Trend ERA5 [K/dec]	
v19	-0.13	$\alpha > 5\%$	-0.08	$\alpha > 30\%$
h19	-0.09	$\alpha > 30\%$	-0.06	$\alpha > 30\%$
v22	-0.10	$\alpha > 30\%$	-0.07	$\alpha > 30\%$
v37	-0.17	$\alpha > 5\%$	-0.08	$\alpha > 30\%$
h37	0.0	$\alpha > 30\%$	0.0	$\alpha > 30\%$
v85	-0.19	$\alpha > 5\%$	0.02	$\alpha > 30\%$
h85	-0.04	$\alpha > 30\%$	0.12	$\alpha > 30\%$
v91			0.15	$\alpha > 5\%$
h91			0.13	$\alpha > 5\%$

	Validation Report Microwave Imager Radiance FCDR R4	Doc. No: SAF/CMDWD/VAL/FCDR_MW Issue: 1.5 Date: 2022-03-31
---	--	--

values are within the optimum and target thresholds (see Table III-2). The long-term trends for the 85 GHz channels are biased by the discontinuity of the transition to SSMIS.

However, the results of this linear trend analysis must be carefully interpreted because the reanalysis is not a stable reference. Observed trends can be caused by the reanalysis or the FCDR data records.

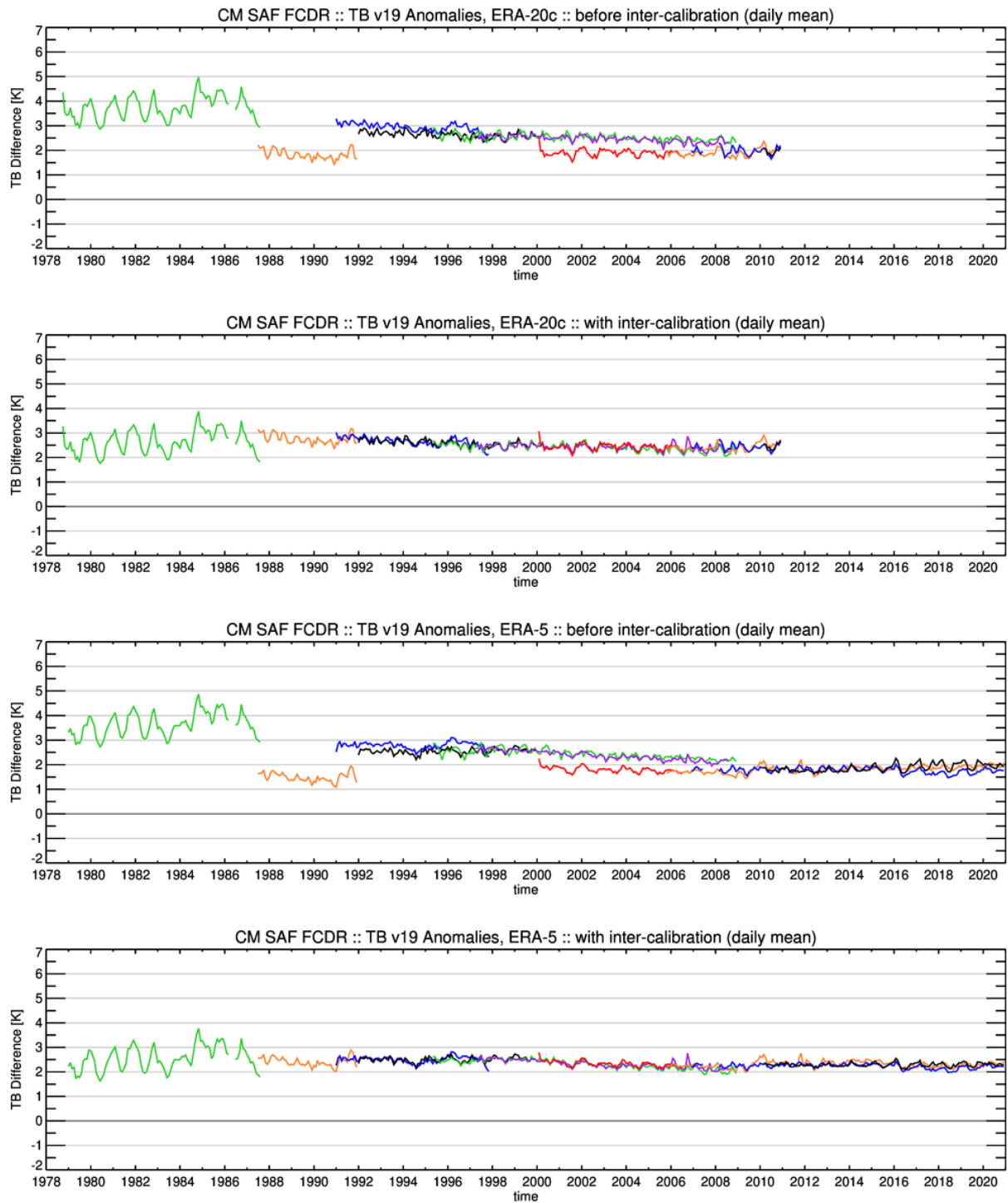


Figure V-1: Time series of global monthly mean TB differences for the 19v GHz channel between the FCDR and ERA 20C (first two panels) and between FCDR and ERA5 (last two panels). Colours for the instrument are SMMR (green), F08 (orange), F10 (blue), F11 (black), F13 (green), F14 (violet), F15 (red), F16 (orange), F17 (blue), F18 (black).

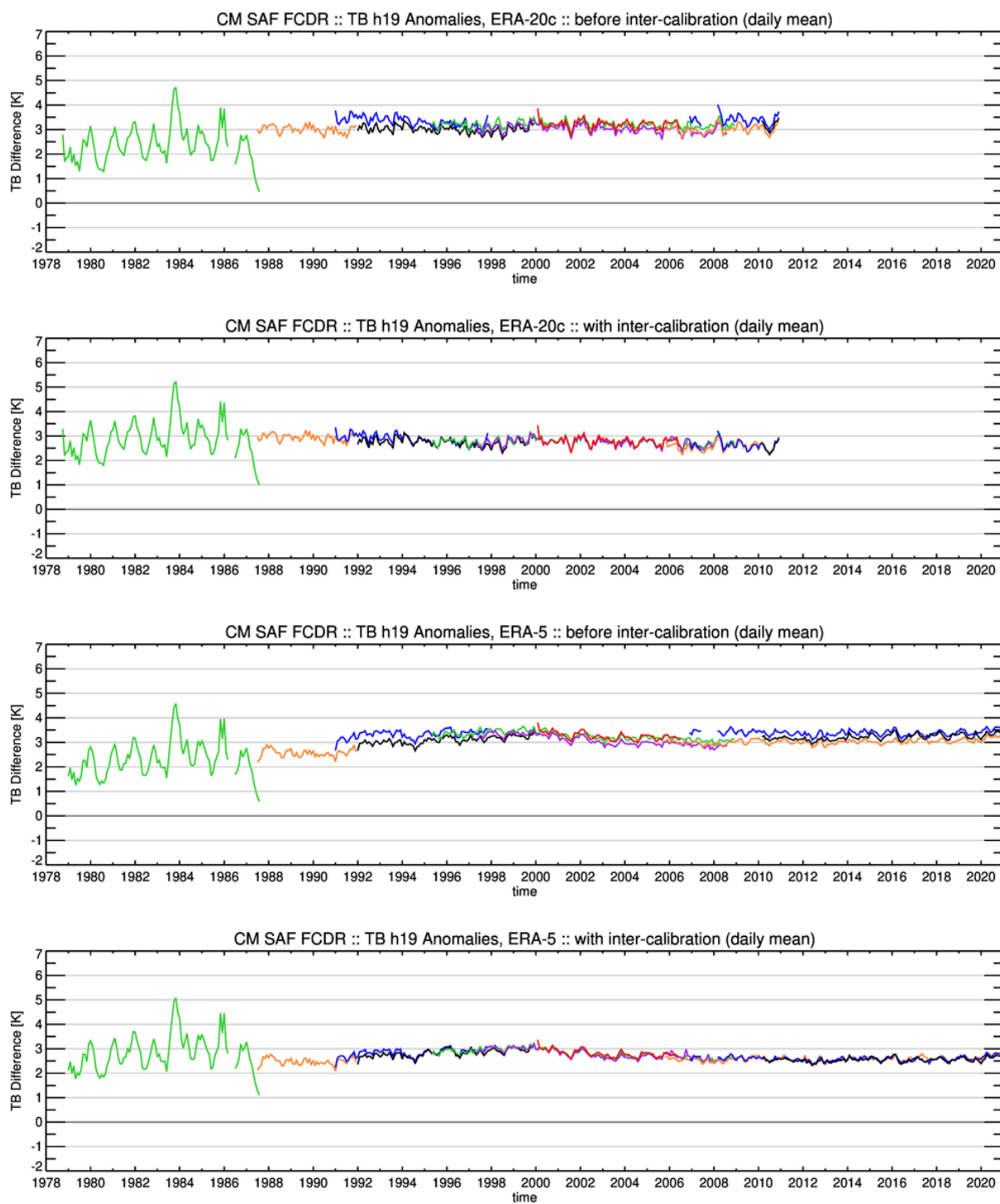


Figure V-2: Same as Figure V-1 but for 19h GHz.

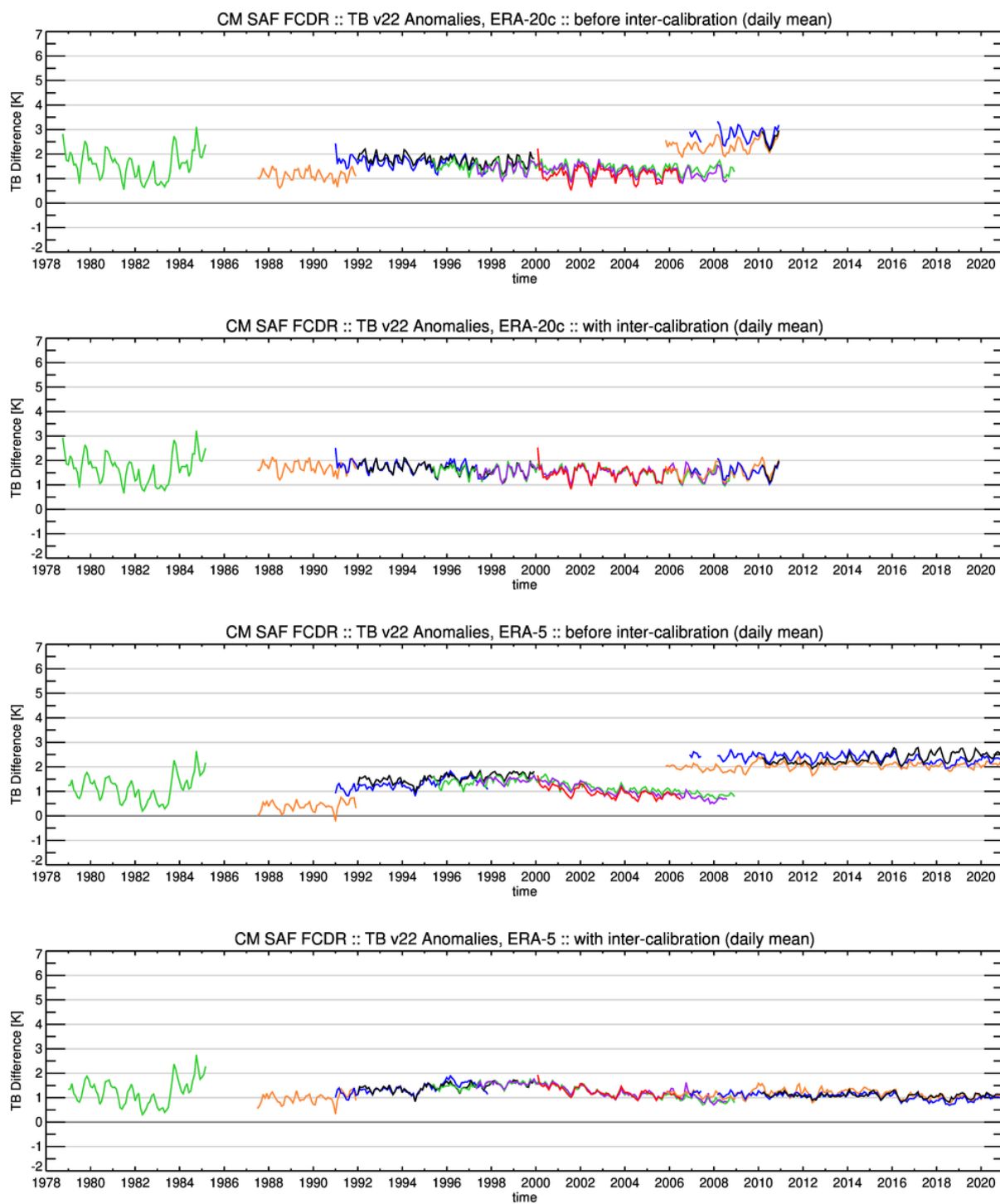


Figure V-3: Same as Figure V-1 but for 22v GHz.

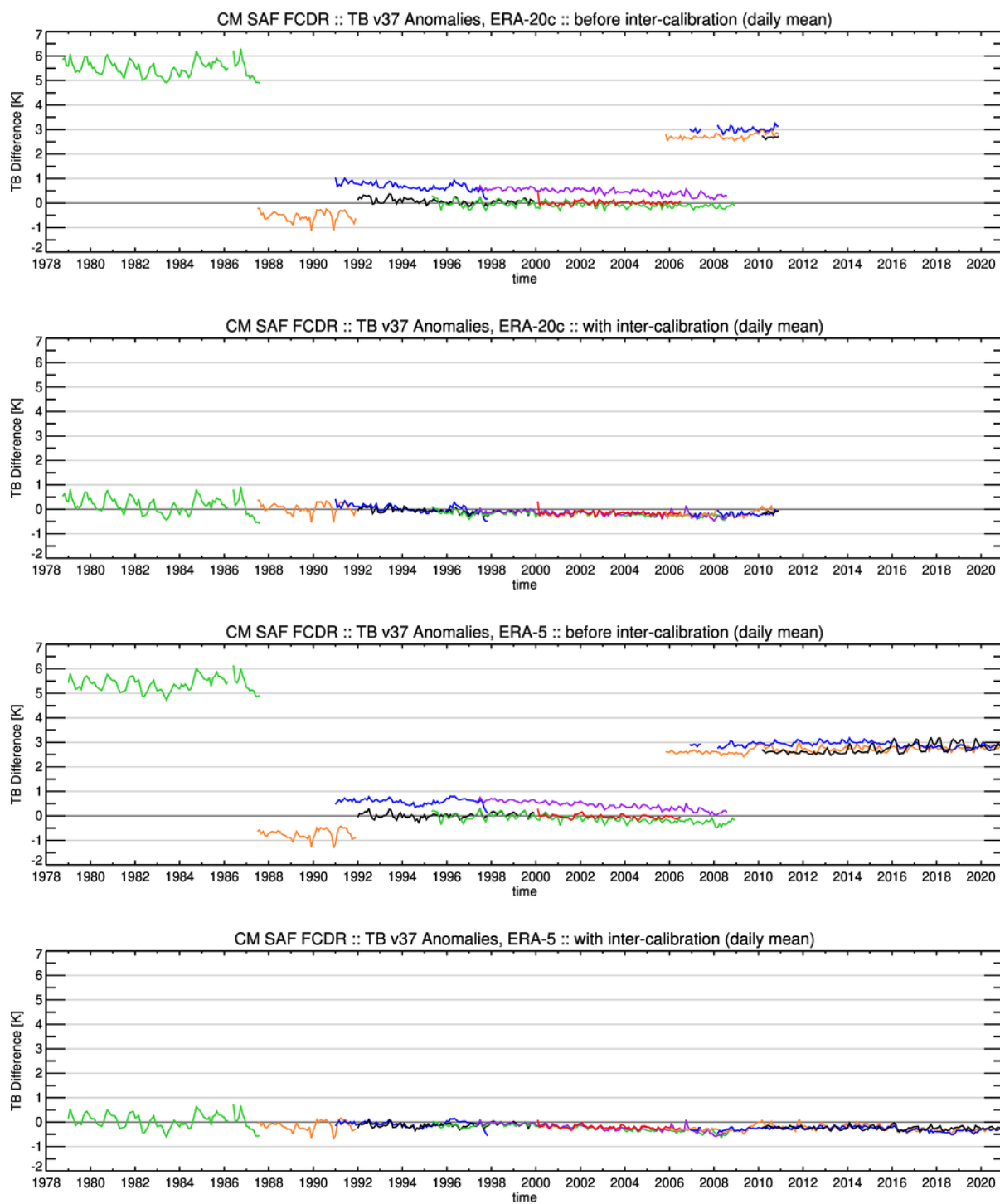


Figure V-4: Same as Figure V-1 but for 37v GHz.

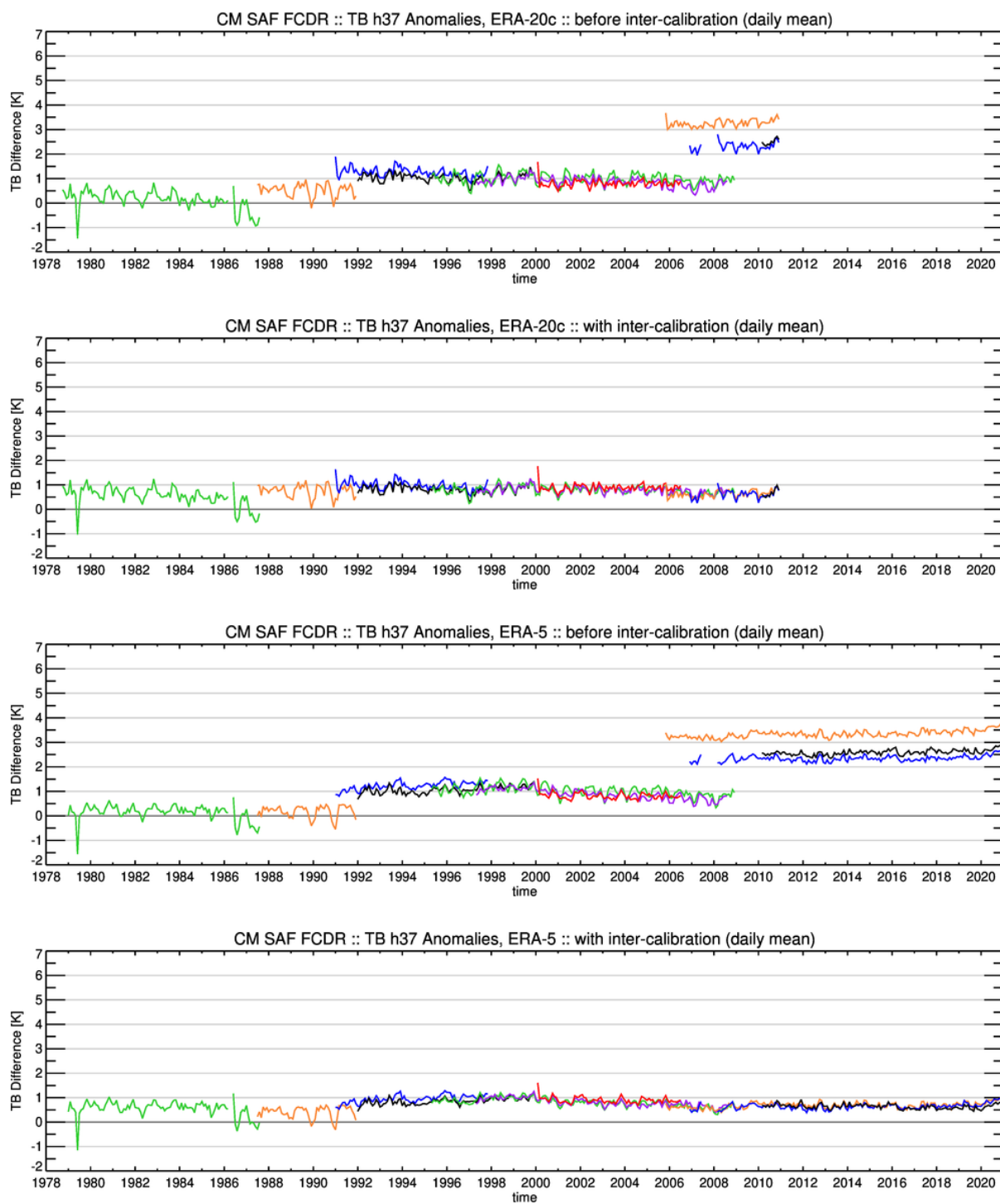


Figure V-5: Same as Figure V-1 but for 37h GHz.

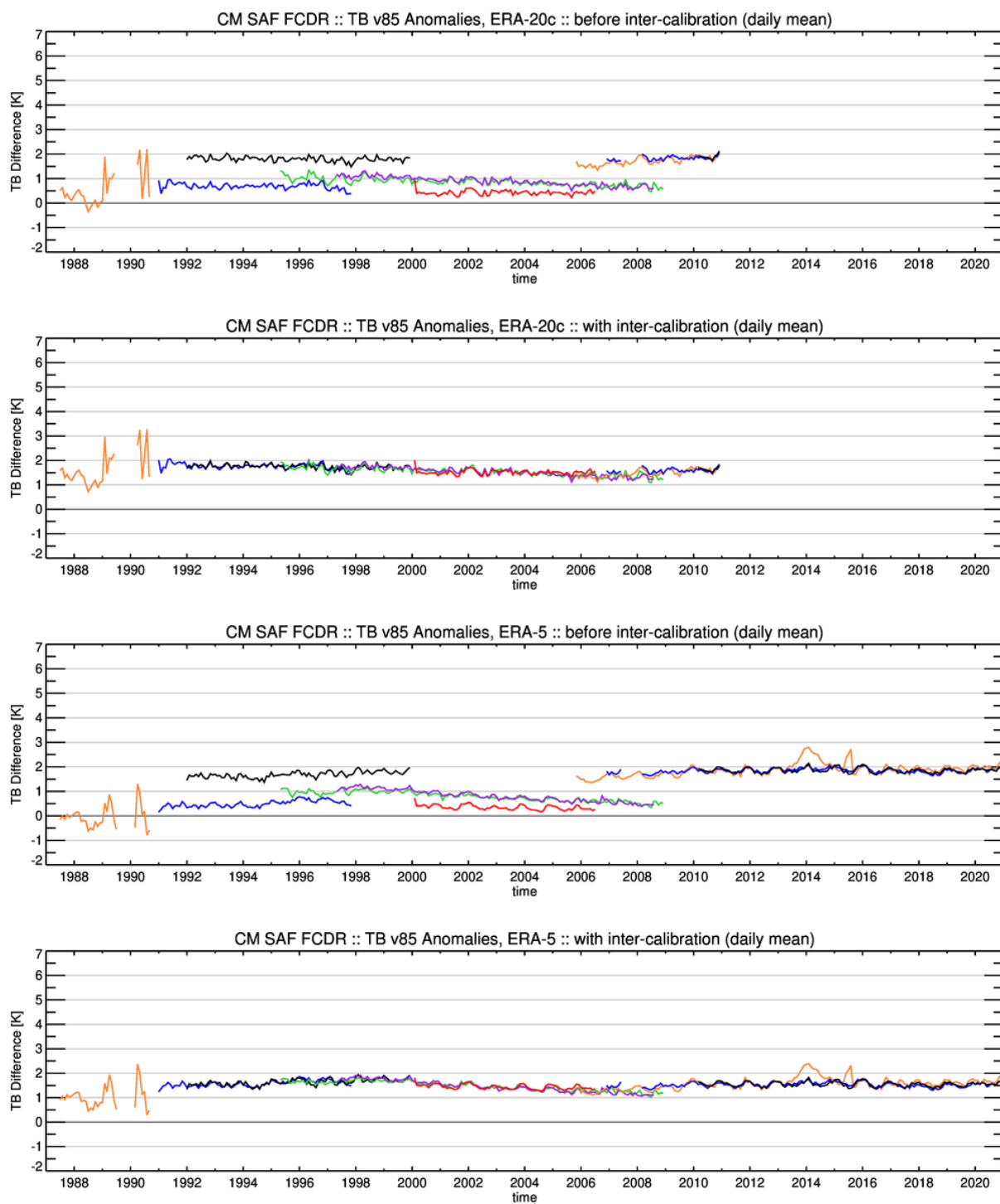


Figure V-6: Same as Figure V-1 but for 85v GHz.

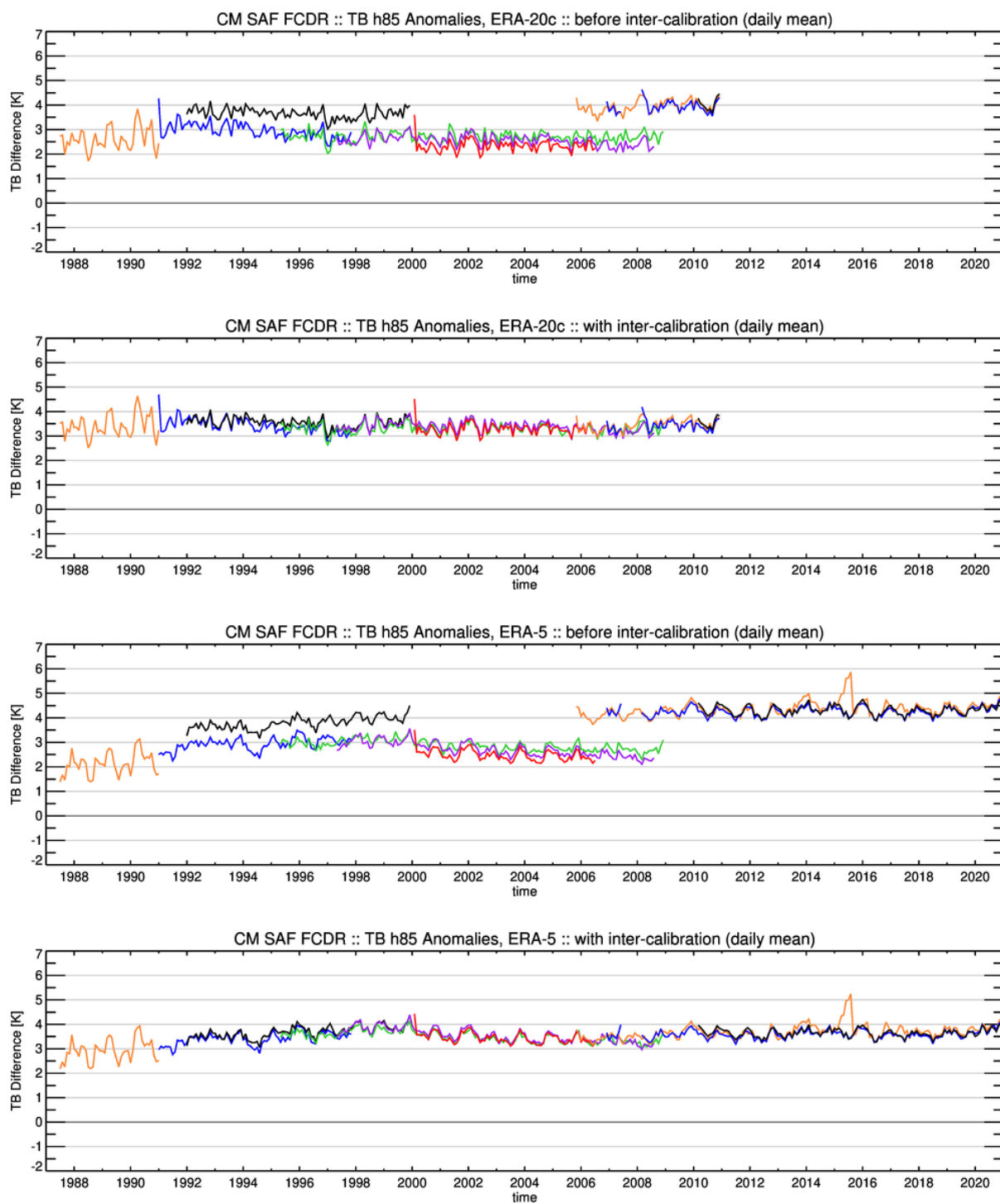


Figure V-7: Same as Figure V-1 but for 85h GHz.

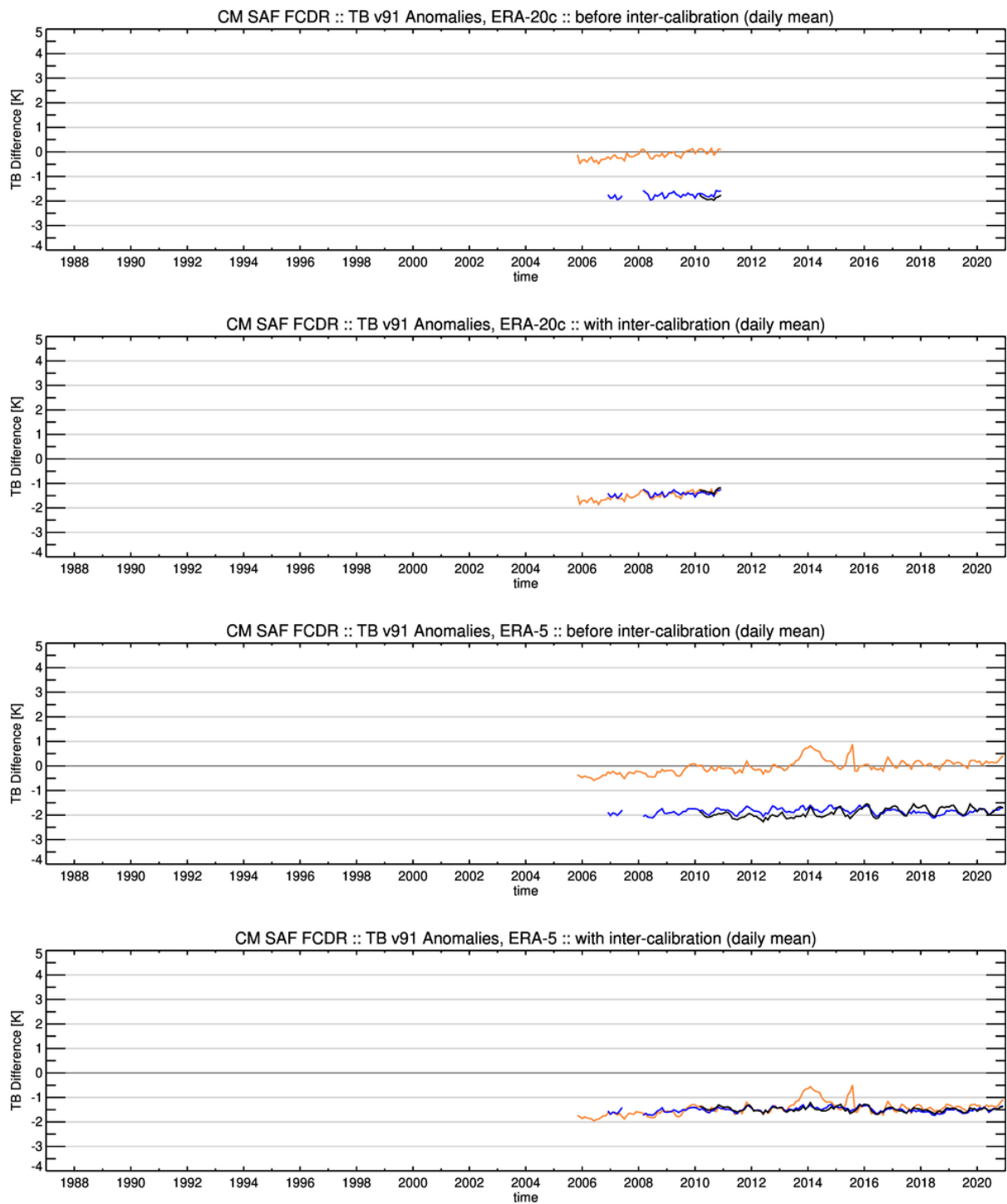


Figure V-8: Same as Figure V-1 but for 91vGHz.

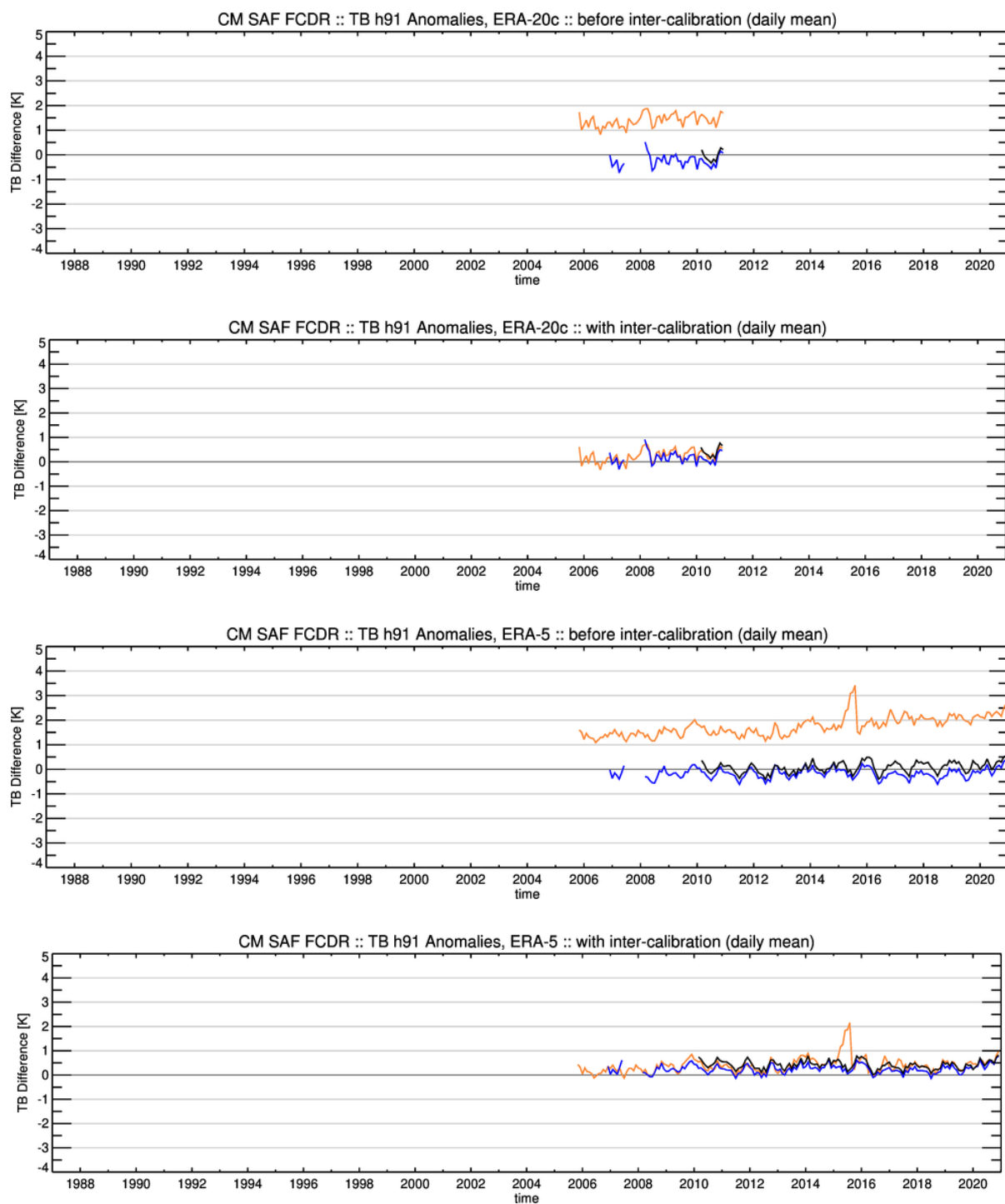


Figure V-9: Same as Figure V-1 but for 91h GHz.

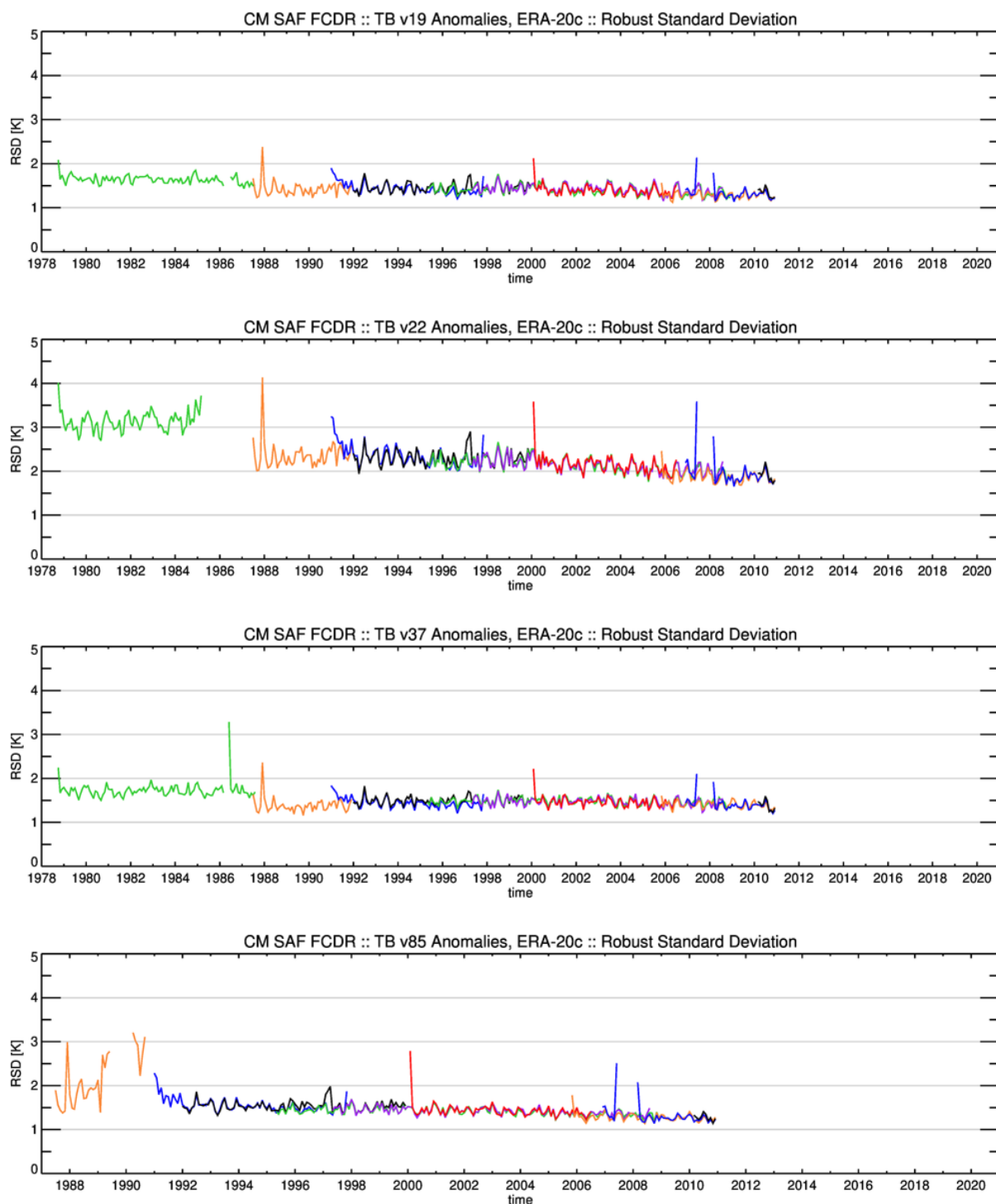


Figure V-10: Time series of robust standard deviation of global monthly mean TB differences for the channels 19v, 22v, 37v, and 85v GHz between the CM SAF FCDR and ERA 20C

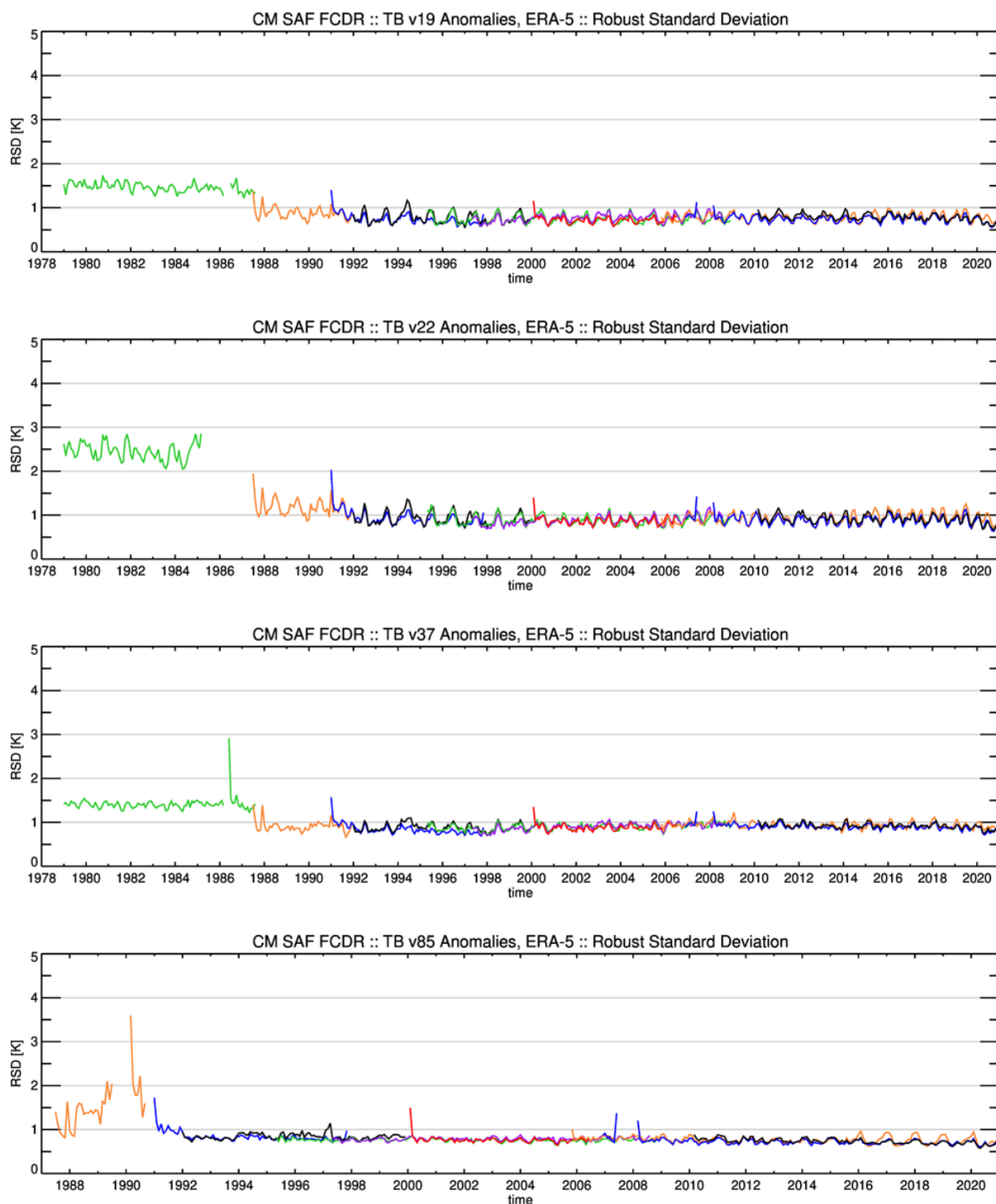


Figure V-11: Time series of robust standard deviation of global monthly mean TB differences for the channels 19v, 22v, 37v, and 85v GHz between the CM SAF FCDR and ERA5.

VI Conclusions

The CM SAF FCDR of SMMR, SSM/I and SSMIS brightness temperatures has been evaluated to analyse the homogeneity, consistency and the stability of the developed inter-calibration model (for SSM/I see RD 4). The CM SAF FCDR has been compared to the original RDR and another available FCDR from CSU. The main distinction between both FCDRs is found in the applied inter-calibration method. The inter-calibration method developed for the CM SAF FCDR explicitly includes all possible surface types to account for the entire natural distribution of brightness temperatures from radiometric cold scenes (rain-free ocean) to radiometric warm scenes (vegetated land surfaces). In contrast to this, the inter-calibration method developed at CSU uses only rain-free brightness temperatures range observed by the TMI instrument because this is used as transfer standard. This limits the CSU inter-calibration to the radiometric cold end of the natural spectrum and hampers a consideration of the full range of possible scene dependencies.

In section III-4.2 it is shown that the CM SAF inter-calibration model is applicable over all surface types. While both evaluated FCDRs show similar characteristics over oceans (radiometric cold scenes), land and sea ice covered areas (radiometric warm scenes) remain biased in the CSU FCDR. As discussed in section III-4.2, polarization double difference maps are used as a cross check to show how the inter-calibration performs for the different surface types. This comparison proves that the CM SAF inter-calibration model leads to an improvement over the CSU FCDR, particular for land and sea ice covered regions, as it better accounts for the strong scene dependent bias of the SSMIS compared to the CSU method: While the CM SAF method removes most of the observed differences over warm scenes, resulting in consistent characteristics in vertically and horizontally polarized channels, the CSU FCDR depicts offsets in the order of up to 2 K after inter-calibration.

The consistency and homogeneity of FCDR and the uncorrected RDR were statistically analysed to demonstrate the improvement of the re-processed data records and compliance with the user requirements. Those requirements are defined in terms of mean absolute systematic inter-satellite deviations and decadal stability. The stability and homogeneity has also been tested by comparing the observed brightness temperatures against GMI observations (SSMIS only) and against modelled brightness temperatures using two different reanalysis products.

The observed differences in the RDR range between 0.5 K to 2.5 K, depending on channel and instrument, but generally the differences are smaller within the SSMIS series as compared to the inter-sensor difference to the SSM/I family. The overall mean differences in the CM SAF FCDR between the different sensors have been reduced to below 0.1 K, which is a significant improvement over the RDR. The mean RSD for all channels and instruments has been significantly reduced. The observed remaining variability in the inter-calibrated TBs is mainly caused by the natural variability due to overpass time differences and sampling differences. No significant trend above 0.03 K/decade can be observed in the intersensor differences.

In section IV-2 the SMMR has been evaluated using ERA-20C as a transfer standard. It was shown, that the global mean anomalies of SMMR and the F08 SSM/I agree well after inter-calibration. The SMMR depicts higher values for the RSD, but still at the same magnitude. This is mainly due to higher *NEdT* values and poorer coverage with a 50% duty cycle.

	<p align="center">Validation Report Microwave Imager Radiance FCDR R4</p>	<p>Doc. No: SAF/CMDWD/VAL/FCDR_MWI Issue: 1.5 Date: 2022-03-31</p>
---	--	--

Comparing the FCDR against modelled brightness temperatures confirmed the results from the inter-sensor differences. However, it is still difficult to interpret the results in terms of temporal stability, as also the reanalysis is not a stable reference. This approach becomes very useful when the overlap period between two instruments is short, like for example F08 to F10. In this case it could be shown that the inter-calibration of the synthetic 85 GHz channels can be improved.

Finally, it can be concluded that this FCDR is providing a greatly improved quality of the SMMR and SSMIS brightness temperatures as compared to original raw data records and fulfils the aimed requirements. It extends the current FCDR until end of 2020. The final combined FCDR provides inter-calibrated brightness temperatures for the time period from 1978 to 2020.

VII References

Andersson, A., Fennig, K., Klepp, C., Bakan, S., Graßl, H., and Schulz, J.: The Hamburg Ocean Atmosphere Parameters and Fluxes from Satellite Data – HOAPS-3, *Earth Syst. Sci. Data*, 2, 215-234, doi:10.5194/essd-2-215-2010, 2010.

Andersson, A., C. Klepp, K. Fennig, S. Bakan, H. Graßl, and J. Schulz: Evaluation of HOAPS-3 ocean surface freshwater flux components, *Journal of Applied Meteorology and Climatology*, 50, 379-398, doi:10.1175/2010JAMC2341.1, 2011.

Berg, W., Sapiano, M. R. P. ; Horsman, J. ; Kummerow, C., 2012: Improved Geolocation and Earth Incidence Angle Information for a Fundamental Climate Data Record of the SSM/I Sensors, *IEEE Transactions on Geoscience and Remote Sensing*, Early online release, doi: 10.1109/TGRS.2012.2199761.

Berg, W., 2013: Fundamental Climate Data Record (FCDR) for the Special Sensor Microwave Imager/Sounder (SSMIS), Climate Algorithm Theoretical Basis Document (C-ATBD), CDR Program Document Number: CDRP-ATBD-0338

Draper, D. W., D. Newell, F. J. Wentz, S. Krimchansky, and G. M. Skofronick-Jackson, 2015: The Global Precipitation Measurement (GPM) Microwave Imager (GMI): Instrument overview and early on-orbit performance. *IEEE Journal of Selected Topics in Applied Earth Observations and Remote Sensing*. doi:10.1109/JSTARS.2015.2403303.

Fennig, K.; Andersson, A.; Schröder, M. (2013): Fundamental Climate Data Record of SSM/I Brightness Temperatures. Satellite Application Facility on Climate Monitoring. DOI:10.5676/EUM_SAF_CM/FCDR_SSMI/V001.

Fennig, K.; Andersson, A.; Schröder, M. (2015): Fundamental Climate Data Record of SSM/I / SSMIS Brightness Temperatures. Satellite Application Facility on Climate Monitoring. DOI:10.5676/EUM_SAF_CM/FCDR_MWI/V002.

Francis, E. A. (1987): Calibration of the Nimbus-7 Scanning Multichannel Microwave Radiometer (SMMR) 1979-1984. Master's Thesis, College of Oceanography, Oregon State University, Corvallis Oregon.

Furhop, R. and Simmer, C.: SSM/I Brightness Temperature Corrections for Incidence Angle Variations, *J. Atmos. Oceanic Technol.*, 13, 246–254, 1996.

Hersbach, H, Bell, B, Berrisford, P, et al. The ERA5 global reanalysis. *Q J R Meteorol Soc.* 2020; 146: 1999– 2049. <https://doi.org/10.1002/qj.3803>

Hollinger, J., Poe, G..A.: Special Sensor Microwave/Imager User's Guide, Naval Research Laboratory Report, Washington DC, 1987.

Njoku, E. G. (2003): Nimbus-7 SMMR Pathfinder Brightness Temperatures, Version 1., Boulder, Colorado USA. NASA National Snow and Ice Data Center Distributed Active Archive Center. DOI:10.5067/7Y1XWXT07HH8.

Poli P, and Co-authors (2013): The data assimilation system and initial performance evaluation of the ECMWF pilot reanalysis of the 20th-century assimilating surface observations only

	Validation Report Microwave Imager Radiance FCDR R4	Doc. No: SAF/CMDWD/VAL/FCDR_MWI Issue: 1.5 Date: 2022-03-31
---	--	---

(ERA-20C). ERA Report Series 14, September 2013, 59 pp., available from ECMWF, Shinfield Park, Reading. <http://old.ecmwf.int/publications/library/do/references/list/782009>

Schröder, M., M. Lockhoff, J. Forsythe, H. Cronk, T. H. Vonder Haar, R. Bennartz, 2016: The GEWEX water vapor assessment (G-VAP) – results from the trend and homogeneity analysis. J. Applied Meteor. Clim., 1633-1649, 55 (7), doi: /10.1175/JAMC-D-15-0304.1.

Semunegus, H: Remote Sensing Systems Version-6 Special Sensor Microwave/Imager Fundamental Climate Data Record, Climate Algorithm Theoretical Basis Document, Climate Data Record (CDR) Program, CDRP-ATBD-0100, 2011.

VIII Glossary

APC	Antenna Pattern Correction
ATBD	Algorithm Theoretical Baseline Document
CM SAF	Satellite Application Facility on Climate Monitoring
CDOP	Continuous Development and Operations Phase
CSU	Colorado State University
DMSP	Defense Meteorological Satellite Program
DWD	Deutscher Wetterdienst (German MetService)
ECI	Earth-centred inertial
ECMWF	European Centre for Medium Range Forecast
ECV	Essential Climate Variable
EIA	Earth Incidence Angle
EPS	European Polar System
ERA-20C	ECMWF Reanalysis of the 20th century
ERA5	ECMWF Reanalysis
EUMETSAT	European Organisation for the Exploitation of Meteorological Satellites
FCDR	Fundamental Climate Data Record
FMI	Finnish Meteorological Institute
FOV	Field of view
GCOS	Global Climate Observing System
GLOBE	The Global Land One-kilometer Base Elevation
HOAPS	The Hamburg Ocean Atmosphere Fluxes and Parameters from Satellite data
IOP	Initial Operations Phase
KNMI	Koninklijk Nederlands Meteorologisch Instituut
MAD	Median absolute deviation
MD5	Message-Digest Algorithm 5
MSG	Meteosat Second Generation
NASA	National Aeronautics and Space Administration

NCEP	National Centers for Environmental Prediction
NDBC	National Data Buoy Center
NESDIS	National Environmental Satellite, Data, and Information System
NMHS	National Meteorological and Hydrological Services
NOAA	National Oceanic & Atmospheric Administration
NWP	Numerical Weather Prediction
PRD	Product Requirement Document
PUM	Product User Manual
QC	Quality Control
RDR	Raw Data Record
RMIB	Royal Meteorological Institute of Belgium
RMS	Root Mean Square
RSD	Robust Standard Deviation
RSS	Remote Sensing Systems
SAF	Satellite Application Facility
SI	Système international d'unités
SMHI	Swedish Meteorological and Hydrological Institute
SMMR	Scanning Multichannel Microwave Radiometer
SMMR	Scanning Multichannel Microwave Radiometer
SSM/I	Special Sensor Microwave Imager
SSMIS	Special Sensor Microwave Imager Sounder
TA	Antenna Temperature
TB	Brightness Temperature
TDR	Temperature Data Records